Gates, States, and Circuits

Notes on the circuit model of quantum computation

Tech. Note 014 v0.5 BETA

http://threeplusone.com/gates

Gavin E. Crooks

2020-11-17

Contents

List of figures 4

List of tables 5

1 Introduction: Gates, states, and circuits 6
- 1.1 Additional reading . . . 6

2 Pauli Group and Pauli Algebra 7

3 Bloch sphere representation of a qubit 8

4 Standard single qubit gates 10
- 4.1 Pauli gates . . . 10
  - Pauli-I gate . . . 10
  - Pauli-X gate . . . 10
  - Pauli-Y gate . . . 11
  - Pauli-Z gate . . . 11
- 4.2 Rotation gates . . . 12
  - R_x gate . . . 12
  - R_y gate . . . 12
  - R_z gate . . . 13
  - Phase shift gate . . . 14
  - $R_{\vec{n}}$ gate . . . 14
- 4.3 Pauli-power gates . . . 16
  - X power gate . . . 16
  - Y power gate . . . 16
  - Z power gate . . . 16
- 4.4 Quarter turns . . . 17
  - V gate . . . 17
  - Inverse V gate . . . 17
  - Pseudo-Hadamard gate . . . 18
  - Inverse pseudo-Hadamard gate . . . 18

S gate . . . 18
Inverse S gate . . . 19
4.5 Hadamard gates . . . 19
Hadamard gate . . . 19
Hadamard-like gates . . . 21
Hadamard power gate . . . 22
4.6 T gates . . . 22
T gate . . . 22
Inverse T gate . . . 23
4.7 Global phase . . . 23
Global phase gate . . . 23
Omega gate . . . 23

5 Decomposition of 1-qubit gates 24
5.1 Bloch rotation decomposition . . . 24
5.2 Z-Y decompositions . . . 24
5.3 ABC decomposition . . . 26
5.4 General Pauli-rotation decompositions . . . 26
5.5 Kronecker decomposition . . . 27

6 The canonical gate 28

7 Standard 2-qubit gates 32
7.1 Clifford gates . . . 32
Identity gate . . . 32
Controlled-NOT gate (CNOT, controlled-X, CX) . . . 32
iSWAP-gate . . . 32
SWAP-gate . . . 32
7.2 XX gates . . . 33
XX gate (Ising) . . . 33
Mølmer-Sørensen gate (MS) . . . 33
Magic gate (M) . . . 33
YY gate . . . 34
ZZ gate . . . 34
Controlled-Y gate . . . 34
Controlled-Z gate . . . 34
Controlled-V gate . . . 35
Barenco gate . . . 35
7.3 XY gates . . . 35
XY-gate . . . 35
Double Controlled NOT gate . . . 35
Givens gate . . . 36
bSWAP (Bell-Rabi) gate . . . 36
Mystery gate . . . 36
Dagwood Bumstead (DB) gate . . . 36
7.4 Exchange-interaction gates . . . 37
EXCH (XXX) gate . . . 37
SWAP-alpha gates . . . 37
$\sqrt{\text{SWAP}}$-gate . . . 37
Inverse $\sqrt{\text{SWAP}}$-gate . . . 37

7.5 Parametric SWAP gates . . . 38
pSwap gate . . . 38
Quantum Fourier transform (QFT) . . . 38
7.6 Orthogonal gates . . . 39
B (Berkeley) gate . . . 39
ECP-gate . . . 40
W-gate . . . 40
7.7 XXY gates . . . 41
FSIM (Ferminoic Simulator) gate . . . 41
Sycamore gate . . . 42

8 Standard 3-qubit gates **43**
Toffoli gate (controlled-controlled-not, CCNOT) . . . 43
Fredkin gate (controlled-swap, CSWAP) . . . 43
CCZ gate (controlled-controlled-Z) . . . 43
Peres gate . . . 44
Deutsch gate . . . 44

9 2-Level Unitary gates **45**
9.1 Two-level unitary decomposition . . . 45
9.2 Control-gate decomposition of 2-level unitary . . . 46

10 Clifford Gates **47**
10.1 Single qubit Clifford gates . . . 47
10.2 Two qubit Clifford gates . . . 48
10.3 Clifford tableau . . . 50
10.4 Generation of Clifford gates . . . 51
10.5 Gottesman–Knill theorem . . . 51
10.6 Decomposition of Clifford gates . . . 51

A Miscellaneous mathematics **52**
A.1 Arctangent . . . 52

B Weyl Chamber **53**

Notes **54**

Bibliography **55**

Index **58**

List of Figures

1 Bloch sphere representation of single qubit states. 8
2 Location of standard basis states on the Bloch sphere. 9
3 Pauli rotations of the Bloch Sphere 13
4 Spherical ball of 1-qubit gates. Each point within this sphere represents a unique 1-qubit gate (up to phase). Antipodal points on the surface represent the same gate. The Pauli rotation gates lie along the three principal axes. 15
5 Coordinates of common 1-qubit gates 15
6 Coordinates of the 6-Hadamard like gates. 21
7 Location of the 11 principal 2-qubit gates in the Weyl chamber. All of these gates have coordinates of the form $\mathsf{CAN}(\frac{1}{4}k_x, \frac{1}{4}k_y, \frac{1}{4}k_z)$, for integer k_x, k_y, and k_z. Note there is a symmetry on the bottom face such that $\mathsf{CAN}(t_x, t_y, 0) \sim \mathsf{CAN}(\frac{1}{2} - t_x, t_y, 0)$. 31
8 The Weyl chamber of canonical non-local 2 qubit gates. (Print, cut, fold, and paste) 53

List of Tables

1 Euler decompositions 26
2 Canonical coordinates of common 2-qubit gates 30
3 Coordinates of the 24 1-qubit Clifford gates. 49
4 Clifford tableaus for 2-qubit gates 50
5 Number of Clifford gates $|C_n|$ for n qubits [1] 51

1 Introduction: Gates, states, and circuits

We shouldn't be asking 1where do quantum speedups come from?' we should say 'all computers are quantum, [...]' and ask 'where do classical slowdowns come from?' — Charlie Bennett [1]

It appears that very rapid progress is now being made on the fundamentals of quantum computing. It is well to keep in mind, though, that many basic issues of the realization of quantum computers remain unsolved or very difficult. — David P. Diviencero [2]

1.1 Additional reading

The canonical textbook for quantum computing and information remains Michael A. Nielsen's and Isaac L. Chuang's classic "Quantum Computation and Quantum Information" (affectionately know as Mike and Ike) [3]. If you have any serious interest in quantum computing, you should own this book[1]. These notes are going to take a different cut through the subject, with more detail in some places, some newer material, but neglecting other areas, since it is not necessary to repeat what Mike and Ike have already so ably covered. John Preskill's lecture notes [4] are another excellent (If perennially incomplete) treatment of the subject.

For a basic introduction to quantum mechanics, see "Quantum Mechanics: The Theoretical Minimum" by Leonard Susskind and Art Friedman [5]. The traditional quantum mechanics textbooks are not so useful, since they tend to rapidly skip over the fundamental and informational aspects, and concentrate on the detailed behavior of light, and atoms, and cavities, and what have you. Such physical details are important if you're building a quantum computer, obviously, but not so much for programming one, and I think the traditional approach tends to obscure the essentials of quantum information and how fundamentally different quantum is from classical physics. But among such physics texts, I'd recommend "Modern Quantum Mechanics" by J. J. Sakurai [6].

For gentler introductions to quantum computing see "Quantum Computing: A Gentle Introduction" by Eleanor G. Rieffel and Wolfgang H. Polak [7]. Another interesting take is "Quantum Country" by Andy Matuschak and Michael Nielsen. This is an online introductory course in quantum computing, with builtin spaced repetition [8]. Scott Aaronson's "Quantum Computing since Democritus" [9] is also a good place to start, particularly for computational complexity theory.

Mathematically, quantum mechanics is mostly applied linear algebra, and you can never go wrong learning more linear algebra. For a good introduction see "No Bullshit Guide to Linear Algebra" by Ivan Savov [10], and for a deeper dive "Linear Algebra Done Right" by Sheldon Axler [11].

For a deep dives into quantum information, both "The Theory of Quantum Information" by John Watrous [12] and "Quantum Information Theory" by Mark M. Wilde [13] are excellent, if weighty, tombs.

And if you have very young children, start them early with Chris Ferrie and whurely's "Quantum Computing for Babies" [14].

2 Pauli Group and Pauli Algebra

Recall the 4 1-qubit Pauli operators: $I = \left[\begin{smallmatrix} 0 & 0 \\ 0 & 1 \end{smallmatrix}\right]$, $X = \left[\begin{smallmatrix} 0 & 1 \\ 1 & 0 \end{smallmatrix}\right]$, $Y = \left[\begin{smallmatrix} 0 & -i \\ i & 0 \end{smallmatrix}\right]$, $Z = \left[\begin{smallmatrix} 1 & 0 \\ 0 & -1 \end{smallmatrix}\right]$.

$$\begin{aligned} X^2 = Y^2 = Z^2 &= I \\ XY = -YX &= iZ \\ ZX = -XZ &= iY \\ YZ = -ZY &= iX \end{aligned} \tag{1}$$

Every pair of Pauli matrices either commutes or anti-commutes.

The *Pauli group* of 1 qubit operators consists of the 4 Pauli operators multiplied by factors of ± 1 or $\pm i$. This extra phase ensures that these 16 elements form a group under matrix multiplication. The Pauli group P_n of n qubit operators contains 4^{n+1} elements is formed from the 4 phase factors and tensor products of 1-qubit Pauli matrices,

$$P_n = \{\pm 1, \pm i\} \times \{I, X, Y, Z\}^{\otimes n} \tag{2}$$

3 Bloch sphere representation of a qubit

[?]

$$|\psi\rangle = \alpha\,|0\rangle + \beta\,|1\rangle\,, \qquad |\alpha|^2 + |\beta|^2 = 1 \tag{3}$$

$$|\psi\rangle = e^{i\gamma}\left(\cos(\tfrac{1}{2}\theta)\,|0\rangle + e^{i\phi}\sin(\tfrac{1}{2}\theta)\,|1\rangle\right) \tag{4}$$

$$|\psi\rangle \simeq \cos(\tfrac{1}{2}\theta)\,|0\rangle + e^{i\phi}\sin(\tfrac{1}{2}\theta)\,|1\rangle \tag{5}$$

$0 \leqslant \theta \leqslant \pi$ and $0 \leqslant \phi < 2\pi$.

$\vec{r} = (\sin\theta\cos\phi,\ \sin\theta\sin\phi,\ \cos\theta)$ on the 3-dimensional unit sphere.

$\lvert 0\rangle$	$\vec{r} = (0, 0, +1)$
$\lvert 1\rangle$	$\vec{r} = (0, 0, -1)$
$\lvert +\rangle = \frac{1}{\sqrt{2}}(\lvert 0\rangle + \lvert 1\rangle)$	$\vec{r} = (+1, 0, 0)$
$\lvert -\rangle = \frac{1}{\sqrt{2}}(\lvert 0\rangle - \lvert 1\rangle)$	$\vec{r} = (-1, 0, 0)$
$\lvert +i\rangle = \frac{1}{\sqrt{2}}(\lvert 0\rangle + i\,\lvert 1\rangle)$	$\vec{r} = (0, +1, 0)$
$\lvert -i\rangle = \frac{1}{\sqrt{2}}(\lvert 0\rangle - i\,\lvert 1\rangle)$	$\vec{r} = (0, -1, 0)$

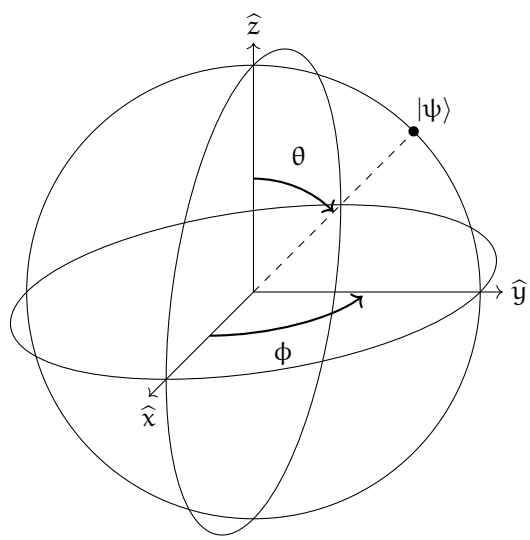

$$|\psi\rangle \simeq \cos(\tfrac{1}{2}\theta)\,|0\rangle + e^{i\phi}\sin(\tfrac{1}{2}\theta)\,|1\rangle$$
$$\vec{r} = (\sin\theta\cos\phi,\ \sin\theta\sin\phi,\ \cos\theta)$$

Figure 1: Bloch sphere representation of single qubit states.

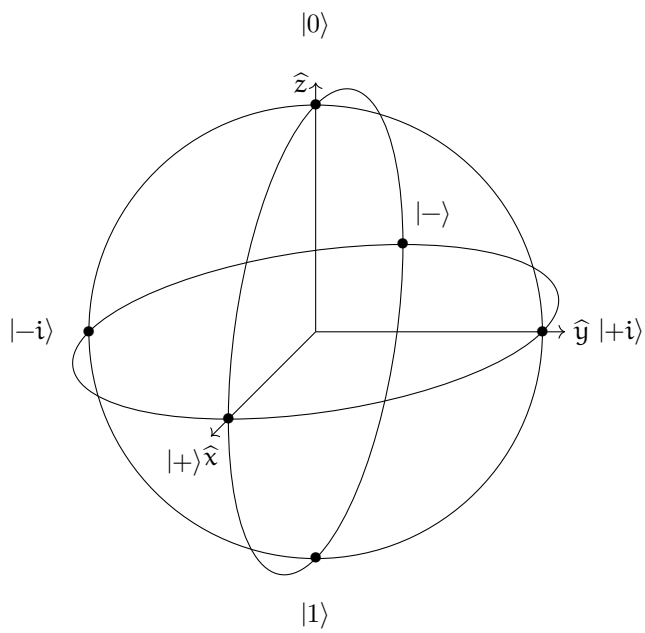

Figure 2: Location of standard basis states on the Bloch sphere.

One-qubit gates rotate the Bloch sphere. Orthogonal states are on opposite sids of the sphere.

4 Standard single qubit gates

Classically, there are only 2 1-bit reversible logic gates, identity and NOT (And 2 irreversible gates, reset to 0 and reset to 1). But in quantum mechanics the zero and one states can be placed into superposition, so there are many other possibilities.

4.1 Pauli gates

The simplest 1-qubit gates are the 4 gates represented by the Pauli operators, I, X, Y, and Z. These operators are also sometimes notated as σ_x, σ_y, σ_z, or with an index σ_i, so that $\sigma_0 = I$, $\sigma_1 = X$, $\sigma_2 = Y$, $\sigma_3 = Z$.

We will explore the algebra of Pauli operators in more detail in chapter **??**. But for now, note that the Pauli gates are all Hermitian, $\sigma_i^\dagger = \sigma_i$, square to the identity $\sigma_i^2 = I$, and that the X, Y, and Z gates anti-commutate with each other.

$$\begin{aligned} XY = -YZ &= iZ \\ YZ = -ZY &= iX \\ ZX = -ZX &= iY \\ XYZ &= iI \end{aligned}$$

Pauli-I gate (identity):

$$I = \begin{bmatrix} 1 & 0 \\ 0 & 1 \end{bmatrix} \tag{6}$$

$$-\boxed{I}-$$

The trivial no-operation gate on 1-qubit, represented by the identity matrix.

$$\begin{aligned} I &= |0\rangle\langle 0| + |1\rangle\langle 1| \\ I\,|0\rangle &= |0\rangle \\ I\,|1\rangle &= |1\rangle \end{aligned}$$

Pauli-X gate (X gate, negation)

$$X = \begin{bmatrix} 0 & 1 \\ 1 & 0 \end{bmatrix} \tag{7}$$

$$-\boxed{X}-$$

The X-gate generates a half-turn in the Bloch sphere about the x axis.

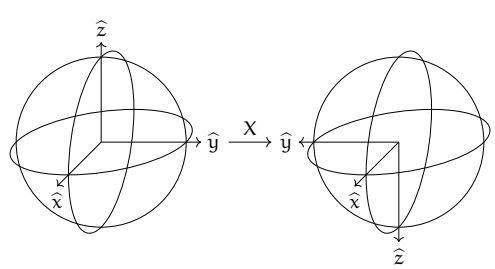

With respect to the computational basis, the X gate is equivalent to a classical NOT operation, or logical negation. The computation basis states are interchanged, so that $|0\rangle$ becomes $|1\rangle$ and $|1\rangle$ becomes $|0\rangle$.

$$\begin{aligned} X &= |1\rangle\langle 0| + |0\rangle\langle 1| \\ X|0\rangle &= |1\rangle \\ X|1\rangle &= |0\rangle \end{aligned}$$

Pauli-Y gate (Y-gate) :

$$Y = \begin{bmatrix} 0 & -i \\ i & 0 \end{bmatrix} \tag{8}$$

$$-\boxed{Y}-$$

A useful mnemonic for remembering where to place the minus sign in the matrix of the Y gate is "Minus eye high" [1]. In some older literature the Y-gate is defined as $iY = \left[\begin{smallmatrix} 0 & 1 \\ -1 & 0 \end{smallmatrix}\right]$ (e.g. [7]), which is the same gate up to a phase.

The Pauli-Y gate generates a half-turn in the Bloch sphere about the $\hat{y}$ axis.

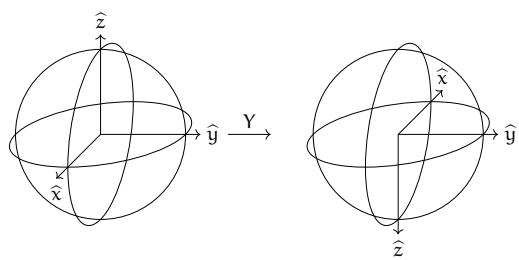

The Y-gate can be thought of as a combination of X and Z gates, $Y = -iZX$. With respect to the computational basis, we interchange the zero and one states and apply a relative phase flip.

$$\begin{aligned} Y &= i|1\rangle\langle 0| - i|0\rangle\langle 1| \\ Y|0\rangle &= +i|1\rangle \\ Y|1\rangle &= -i|0\rangle \end{aligned}$$

Pauli-Z gate (Z-gate, phase flip)

$$Z = \begin{bmatrix} 1 & 0 \\ 0 & -1 \end{bmatrix} \tag{9}$$

$$-\boxed{Z}-$$

$$H_Z = -\pi\tfrac{1}{2}(1 - Z) \tag{10}$$

The Pauli-Z gate generates a half-turn in the Bloch sphere about the $\hat{z}$ axis.

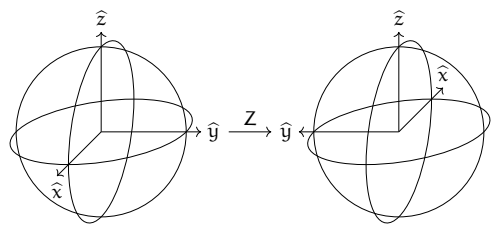

With respect to the computational basis, the Z gate flips the phase of the $|1\rangle$ state relative to the $|0\rangle$ state.

$$
\begin{aligned}
Z &= |0\rangle\langle 0| - |1\rangle\langle 1| \\
Z\,|0\rangle &= +\,|0\rangle \\
Z\,|1\rangle &= -\,|1\rangle
\end{aligned}
$$

4.2 Rotation gates

The three Pauli-rotation gates rotate the state vector by an arbitrary angle about the corresponding axis in the Bloch sphere, Fig. **??**. They are generated by taking exponentials of the Pauli operators. (Recall that $\exp(i\theta A) = \cos(\theta)I + i\sin(\theta)A$ for operators A that square to the identity $A^2 = I$.) [2]

R_x gate [15] Rotate θ radians anti-clockwise about the $\hat{x}$ axis of the Bloch sphere.

$$
\begin{aligned}
R_x(\theta) &= e^{-i\frac{1}{2}\theta X} \\
&= \cos(\tfrac{1}{2}\theta)I - i\sin(\tfrac{1}{2}\theta)X \\
&= \begin{bmatrix} \cos(\frac{1}{2}\theta) & -i\sin(\frac{1}{2}\theta) \\ -i\sin(\frac{1}{2}\theta) & \cos(\frac{1}{2}\theta) \end{bmatrix}
\end{aligned}
\tag{11}
$$

$$-\boxed{R_x(\theta)}-$$

$$-\boxed{R_x(\theta_0)}-\boxed{R_x(\theta_1)}- \;=\; -\boxed{R_x(\theta_0+\theta_1)}-$$

R_y gate [15] Rotate θ radians anti-clockwise about the $\hat{y}$ axis of the Bloch sphere.

$$
\begin{aligned}
R_y(\theta) &= e^{-i\frac{1}{2}\theta Y} \\
&= \cos(\tfrac{1}{2}\theta)I - i\sin(\tfrac{1}{2}\theta)Y \\
&= \begin{bmatrix} \cos(\frac{1}{2}\theta) & -\sin(\frac{1}{2}\theta) \\ \sin(\frac{1}{2}\theta) & \cos(\frac{1}{2}\theta) \end{bmatrix}
\end{aligned}
\tag{12}
$$

$$-\boxed{R_y(\theta)}-$$

Rotate the state vector θ radians anti-clockwise about the $\hat{y}$ axis of the Bloch sphere.

$$-\boxed{R_y(\theta_0)}-\boxed{R_y(\theta_1)}- \;=\; -\boxed{R_y(\theta_0+\theta_1)}-$$

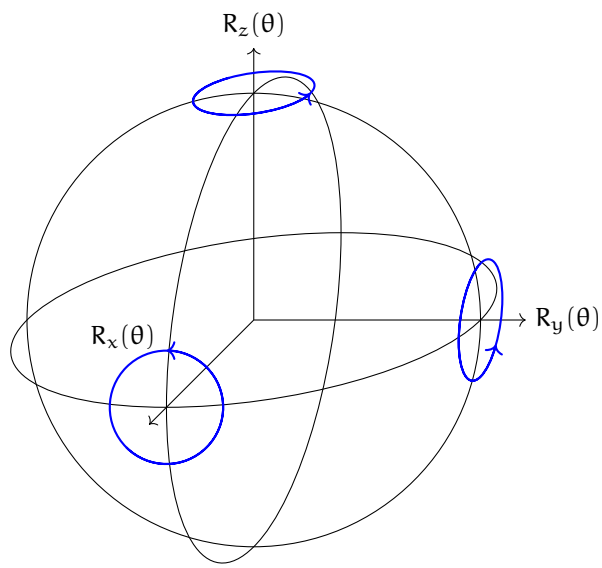

Figure 3: Pauli rotations of the Bloch Sphere

R_z gate [15] Rotate θ radians clockwise about the $\hat{z}$ axis of the Bloch sphere.

$$\begin{aligned} R_z(\theta) &= e^{-i\frac{1}{2}\theta Z} \\ &= \cos(\tfrac{1}{2}\theta)I - i\sin(\tfrac{1}{2}\theta)Z \\ &= \begin{bmatrix} e^{-i\frac{1}{2}\theta} & 0 \\ 0 & e^{+i\frac{1}{2}\theta} \end{bmatrix} \end{aligned} \tag{13}$$

$$-\boxed{R_z(\theta)}-$$

$$-\boxed{R_z(\theta_0)}-\boxed{R_z(\theta_1)}- \;=\; -\boxed{R_z(\theta_0+\theta_1)}-$$

Let us demonstrate that the R_z gate generates rotations about the z axis. Recall the definition of the Boch vector of an arbitrary state ketψ, REF.

$$\begin{aligned} R_z(\theta')\,|\psi\rangle &= \left(e^{-i\frac{1}{2}\theta'}\,|0\rangle\langle 0| + e^{+i\frac{1}{2}\theta'}\,|1\rangle\langle 1|\right)\left(\cos(\tfrac{1}{2}\theta)\,|0\rangle + e^{i\phi}\sin(\tfrac{1}{2}\theta)\,|1\rangle\right) \\ &= e^{-i\frac{1}{2}\theta'}\left(\cos(\tfrac{1}{2}\theta)\,|0\rangle + e^{i(\theta'+\phi)}\,|1\rangle\right) \\ &\simeq \cos(\tfrac{1}{2}\theta)\,|0\rangle + e^{i(\theta'+\phi)}\,|1\rangle \end{aligned} \tag{14}$$

In the last line we drop an irrelevant phase. We can see that the R_z gate has left the elevation angle unchanged, but added θ' to the azimuth angle, which corresponds to a rotation about the z axis.

We can do the same exercise for the R_X and R_Y gates, although the trigonometry is slightly more involved.

Phase shift gate An alternative parameterization of the R_z, from which this gate differs by only a phase.

$$\begin{aligned} R_\phi &= \begin{bmatrix} 1 & 0 \\ 0 & e^{\phi} \end{bmatrix} \\ &= e^{-\frac{1}{2}\phi}\, R_z(\phi) \end{aligned} \tag{15}$$

The name arrises because this gate shifts the phase of the $|1\rangle$ state relative to the $|0\rangle$ state. Sometimes favored over the R_z gate because special values are exactly equal to various other common gates. For instance, $R_\pi = Z$, but $R_z(\pi) = -iZ$.

$R_{\vec{n}}$ gate Rotate θ radians anti-clockwise about an arbitrary axis in the Bloch sphere.

$$\begin{aligned} R_{\vec{n}}(\theta) &= e^{-i\frac{1}{2}\theta(n_x X + n_y Y + n_z Z)} \\ &= \cos(\tfrac{1}{2}\theta) I - i\sin(\tfrac{1}{2}\theta)(n_x X + n_y Y + n_z Z) \\ &= \begin{bmatrix} \cos(\frac{1}{2}\theta) - in_z \sin(\frac{1}{2}\theta) & -n_y \sin(\frac{1}{2}\theta) - in_x \sin(\frac{1}{2}\theta) \\ n_y \sin(\frac{1}{2}\theta) - in_x \sin(\frac{1}{2}\theta) & \cos(\frac{1}{2}\theta) + in_z \sin(\frac{1}{2}\theta) \end{bmatrix} \end{aligned} \tag{16}$$

$$-\boxed{R_{\vec{n}}(\theta)}-$$

Clearly, the Pauli rotation gates are special cases of the general rotation gate.

$$\begin{aligned} R_x(\theta) &= R_{\vec{n}}(\theta), \quad \vec{n} = (1,0,0) \\ R_y(\theta) &= R_{\vec{n}}(\theta), \quad \vec{n} = (0,1,0) \\ R_z(\theta) &= R_{\vec{n}}(\theta), \quad \vec{n} = (0,0,1) \end{aligned}$$

In fact every 1-qubit gate can be represented as a rotation gate (up to phase) with some coordinate $(\theta\, n_x, \theta\, n_y, \theta\, n_z)$, where each axis runs between π and $-\pi$. See figures **??** and **??**.

You might reasonably be wondering why there is a factor of half in the definitions of the rotation gates. A 1-qubit gate is represented by an element of group $SU(2)$, which are rotations in a 2-dimensional complex vector space. But we are visualizing the effect of these gates as rotations in 3-dimensional Euclidean space. These spacial rotations are elements of the special orthogonal gate $SO(3)$. But there is an accidental correspondence between these two groups. We can map two elements of $SU(2)$ (differing by only a -1 phase) to each element of $SO(3)$ while keeping the group structure. In the jargon, $SU(2)$ is a double cover of $SO(3)$. This correspondence is what allows us to visulize 1-qubit gates as rotations in 3-space. But because of this doubling up, a rotation of θ radians in the Bloch sphere corresponds to a rotation of only $\frac{1}{2}\theta$ in the complex vector space. We have to go twice around the Bloch sphere, $\theta = 4\pi$, to get back to the same gate with the same phase.

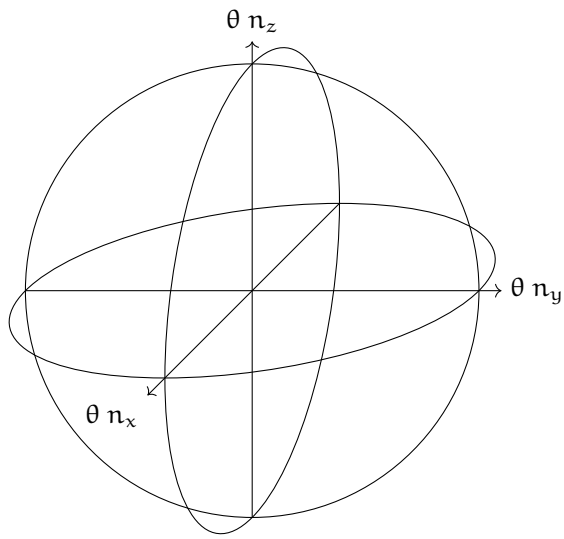

Figure 4: Spherical ball of 1-qubit gates. Each point within this sphere represents a unique 1-qubit gate (up to phase). Antipodal points on the surface represent the same gate. The Pauli rotation gates lie along the three principal axes.

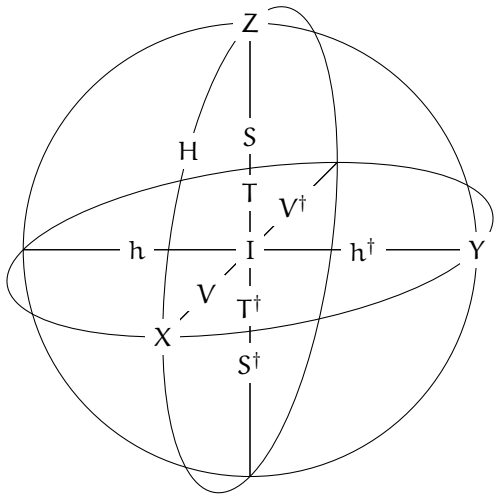

Figure 5: Coordinates of common 1-qubit gates

4.3 Pauli-power gates

It turns out to be useful to define powers of the Pauli-gates. This is slightly tricky because non-integer powers of matrixes aren't unique. Just as there are 2-square roots of any number, a diagonalizable matrix with n unique eigenvalue has 2^n unique square roots. We circumvent this ambiguity by defining the Pauli power gates via the Pauli rotation gates. We note that a π rotation is a Pauli gate up to phase, e.g.

$$R_X(\pi) = e^{-i\frac{\pi}{2}X} = e^{-i\frac{\pi}{2}}X??? \tag{17}$$

and define powers of the Pauli matrices as

$$X^t = e^{-i\frac{\pi}{2}t(X-I)} \simeq R_x(\pi t)\ , \tag{18}$$

and similarly for Y and Z rotations. With this definitions the Pauli-power gates spin states in the same direction around the Bloch sphere as the Pauli-rotation gates.

The Pauli rotation-representation is more natural from the point of view of pure mathematics. But the Pauli-power representation has computational advantages. In quantum circuits we most often encounter rotations of angles $\pm\pi/2^n$ for some integer n. Whereas it is easy to spot that $Z^{0.125}$ is a T gate, for example, it is less obvious that $R_z(0.78538\ldots)$ is the same gate up to phase. Moreover binary fractions have exact floating point representations, whereas fractions of π inevitably suffer from numerical round-off error.

X power gate

$$\begin{aligned} X^t &= e^{-i\frac{\pi}{2}t(X-I)} = e^{i\frac{\pi}{2}t}R_x(\pi t) \\ &= e^{i\frac{\pi}{2}t}\begin{bmatrix} \cos(\frac{\pi}{2}t) & -i\sin(\frac{\pi}{2}t) \\ -i\sin(\frac{\pi}{2}t) & \cos(\frac{\pi}{2}t) \end{bmatrix} \end{aligned} \tag{19}$$

$$-\boxed{X^t}-$$

Y power gate

$$\begin{aligned} Y^t &= e^{-i\frac{\pi}{2}t(Y-I)} = e^{i\frac{\pi}{2}t}R_y(\pi t) \\ &= e^{i\frac{\pi}{2}t}\begin{bmatrix} \cos(\frac{\pi}{2}t) & -\sin(\frac{\pi}{2}t) \\ \sin(\frac{\pi}{2}t) & \cos(\frac{\pi}{2}t) \end{bmatrix} \end{aligned} \tag{20}$$

$$-\boxed{Y^t}-$$

Z power gate

$$\begin{aligned} Z^t &= e^{-i\frac{\pi}{2}t(Z-I)} = e^{i\frac{\pi}{2}t}R_z(\pi t) \\ &= e^{i\frac{\pi}{2}t}\begin{bmatrix} e^{-i\frac{\pi}{2}t} & 0 \\ 0 & e^{+i\frac{\pi}{2}t} \end{bmatrix} = \begin{bmatrix} 1 & 0 \\ 0 & e^{+i\pi t} \end{bmatrix} \end{aligned} \tag{21}$$

$$-\boxed{Z^t}-$$

4.4 Quarter turns

V gate [1, 1] Square root of the X-gate, $VV = X$.

$$\begin{aligned} V &= X^{\frac{1}{2}} \\ &= \tfrac{1}{2}\begin{bmatrix} 1+i & 1-i \\ 1-i & 1+i \end{bmatrix} \\ &= HSH \\ &\simeq R_x(+\tfrac{\pi}{2}) \end{aligned} \tag{22}$$

$$-\boxed{V}- \quad \text{or} \quad -\boxed{X^{\frac{1}{2}}}-$$

A quarter turn anti-clockwise about the $\hat{x}$ axis.

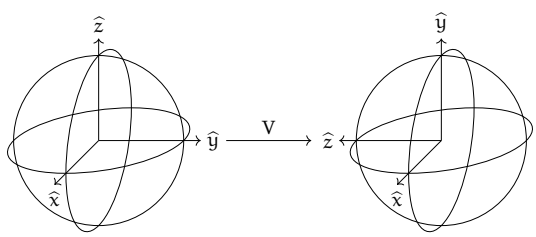

Inverse V gate Since the V-gate isn't Hermitian, the inverse gate, $V^\dagger$, is a distinct square root of X.

$$\begin{aligned} V^\dagger &= X^{-\frac{1}{2}} \\ &= \tfrac{1}{2}\begin{bmatrix} 1-i & 1+i \\ 1+i & 1-i \end{bmatrix} \\ &= HS^\dagger H \\ &\simeq R_x(-\tfrac{\pi}{2}) \end{aligned} \tag{23}$$

$$-\boxed{V^\dagger}- \quad \text{or} \quad -\boxed{X^{-\frac{1}{2}}}-$$

A quarter turn clockwise about the $\hat{x}$ axis.

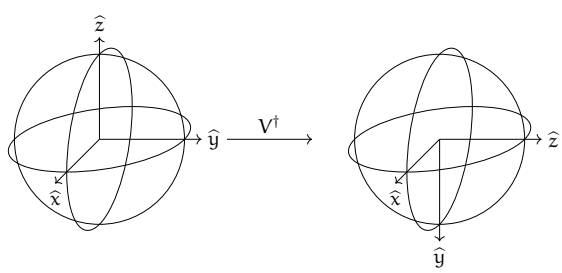

Pseudo-Hadamard gate [16?] .

$$\begin{aligned} \mathsf{h} &= \tfrac{\sqrt{2}}{1+i} \mathsf{Y}^{-\frac{1}{2}} \\ &= \tfrac{1}{\sqrt{2}} \begin{bmatrix} 1 & 1 \\ -1 & 1 \end{bmatrix} \end{aligned} \tag{24}$$

$$-\boxed{\mathrm{Ph}(\alpha)}- \quad \text{or} \quad -\boxed{\mathsf{Y}^{-\frac{1}{2}}}-$$

A quarter turn clockwise about the $\hat{y}$ axis.

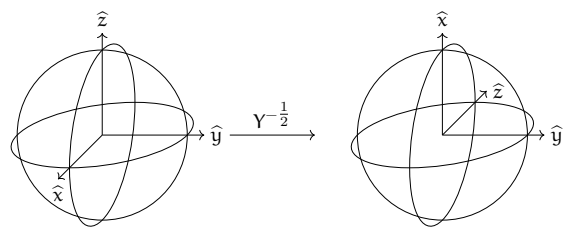

This square-root of the Y-gate is called the pseudo-Hadamard gate as it has the same effect on the computational basis as the Hadamard gate.

$$\begin{aligned} \mathsf{h}\,|0\rangle &= |+\rangle \\ \mathsf{h}\,|1\rangle &= |-\rangle \end{aligned}$$

Inverse pseudo-Hadamard gate Unlike the Hadamard gate, the pseudo-Hadamard gate is not Hermitian, and therefore not its own inverse.

$$\begin{aligned} \mathsf{h}^\dagger &= \frac{1}{\sqrt{2}} \begin{bmatrix} 1 & -1 \\ 1 & 1 \end{bmatrix} \\ &= \tfrac{\sqrt{2}}{1+i} \mathsf{Y}^{\frac{1}{2}} \end{aligned} \tag{25}$$

$$-\boxed{\mathsf{h}^\dagger}- \quad \text{or} \quad -\boxed{\mathsf{Y}^{\frac{1}{2}}}-$$

A quarter turn anti-clockwise about the $\hat{y}$ axis.

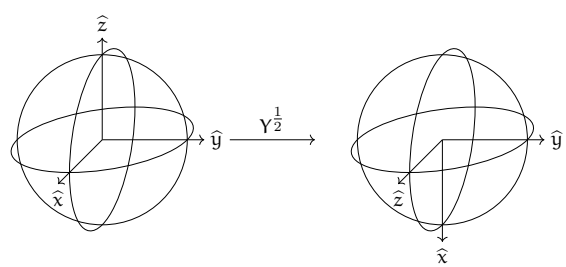

S gate (Phase, P, "ess") Square root of the Z-gate, $\mathsf{SS} = \mathsf{Z}$.

$$\begin{aligned} \mathsf{S} &= \mathsf{Z}^{\frac{1}{2}} \\ &= \begin{bmatrix} 1 & 0 \\ 0 & i \end{bmatrix} \\ &\simeq \mathsf{R}_z(+\tfrac{\pi}{2}) \end{aligned} \tag{26}$$

$$-\boxed{S}-$$

Historically called the phase gate (and denoted by P), since it shifts the phase of the one state relative to the zero state. This is a bit confusing because we have to make the distinction between the phase gate and applying a global phase. Often referred to as simple the S ("ess") gate in contemporary discourse.

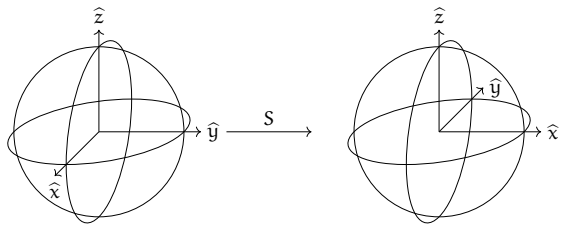

Inverse S gate Hermitian conjugate of the S gate, and an alternative square-root of Z, $S^\dagger S^\dagger = Z$.

$$\begin{aligned} S^\dagger &= Z^{-\frac{1}{2}} \\ &= \begin{bmatrix} 1 & 0 \\ 0 & -i \end{bmatrix} \\ &\simeq R_z(-\tfrac{\pi}{2}) \end{aligned} \tag{27}$$

$$-\boxed{S^\dagger}-$$

A quarter turn clockwise about the $\hat{z}$ axis.

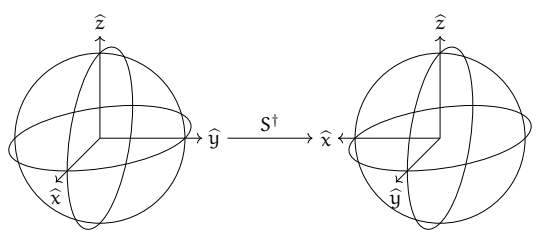

Can be generated from the S gate, $SSS = S^\dagger$.

4.5 Hadamard gates

Hadamard gate The Hadamard gate is one of the most interesting and useful of the common gates. Its effect is a π rotation in the Bloch sphere about the axis $\frac{1}{\sqrt{2}}(\hat{x} + \hat{z})$, essentially half way between the Z and X gates (Fig. 4).

$$\begin{aligned} H &= \tfrac{1}{\sqrt{2}} \begin{bmatrix} 1 & 1 \\ 1 & -1 \end{bmatrix} \\ &\simeq R_{\vec{n}}(\pi), \quad \vec{n} = \tfrac{1}{\sqrt{2}}(1, 0, 1) \end{aligned} \tag{28}$$

$$-\boxed{H}-$$

In terms of the Bloch sphere, the Hadamard gate interchanges the x and y axes, and inverts the y axis.

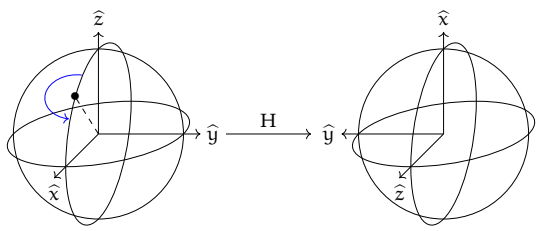

It is also worth noting that a Hadamard similarity transform interchanges X and Z gates,

$$HXH = Z, \qquad HYH = -Y, \qquad HZH = X$$
$$HR_x(\theta)H = R_z(\theta), \qquad HR_y(\theta)H = R_y(-\theta), \qquad HR_z(\theta)H = R_x(\theta)$$

One reason that the Hadamard gate is so useful is that it acts on the computation basis states to create superpositions of zero and one states. These states are common enough that they have their own notation, $|+\rangle$ and $|-\rangle$.

$$H|0\rangle = \tfrac{1}{\sqrt{2}}(|0\rangle + |1\rangle) = |+\rangle$$
$$H|1\rangle = \tfrac{1}{\sqrt{2}}(|0\rangle - |1\rangle) = |-\rangle$$

The square of the Hadamard gate is the identity $HH = I$. This is easy to show with some simple algebra, or by considering that the Hadamard is a 180 degree rotation in the Bloch sphere, or by noting that the Hadamard matrix is both Hermitian and unitary, so the Hadamard must be its own inverse. As a consequence, the Hadamard converts the $|+\rangle$, $|-\rangle$ Hadamard basis back to the $|0\rangle$, $|1\rangle$ computational basis.

$$H|+\rangle = |0\rangle$$
$$H|-\rangle = |1\rangle$$

The Hadamard gate is named for the *Hadamard transform* (Or *Walsh-Hadamard transform*), which in the context of quantum computing is the simultaneous application of Hadamard gates to multi-qubits. We will return this transform presently .

It is also worth noting a couple useful decompositions (up to phase).

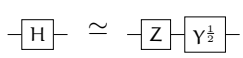

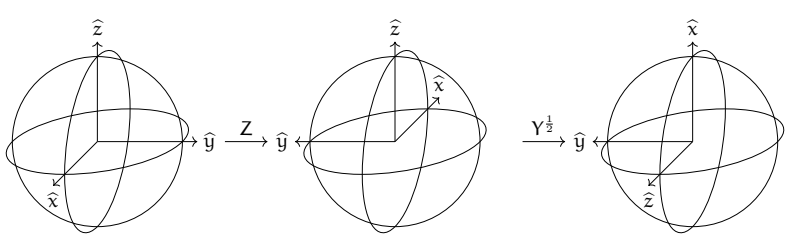

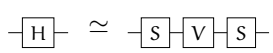

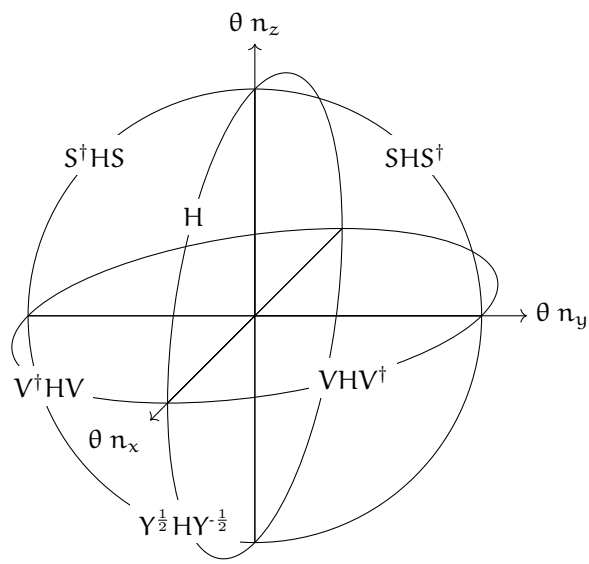

Figure 6: Coordinates of the 6-Hadamard like gates.

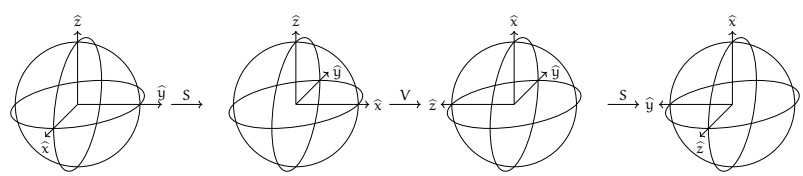

Here, V is the square-root of the X gate, and S is the square-root of Z, each of which is a quarter turn in the Bloch sphere.

Hadamard-like gates If we peruse the sphere of 1-qubit gates, Fig. 4, we can see that there are 6 different Hadamard-like gates that lie between the main $\hat{x}$, $\hat{y}$, $\hat{z}$ axes. (Recall that gates on opposite sides of the sphere's surface are the same up to phase.) Each of these gates can be obtained from straightforward transform so the Hadamard gate. For instance, $SHS^\dagger$ is the Hadamard-like gate between the Z and Y gates, which interchanges the y and z axis, and flips the x-axis.

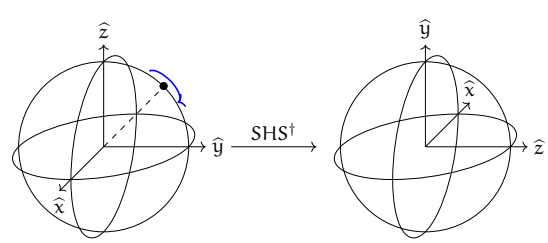

This particular Hadamard-like gate takes the computational Z-basis to the Y-basis.

$$SHS^\dagger |0\rangle = \tfrac{1}{\sqrt{2}}(|0\rangle + i\,|1\rangle) = |{+i}\rangle$$
$$SHS^\dagger |1\rangle = \tfrac{1}{\sqrt{2}}(|0\rangle - i\,|1\rangle) = |{-i}\rangle$$

The coordinates of all 6 Hadamard-like gates are shown in Fig. **??**, and listed in Table **??** in the same block as the Hadamard gate.

Hadamard power gate

$$H_H = \frac{\pi}{2}\left(\frac{1}{\sqrt{2}}(X+Z) - I\right) \tag{29}$$

$$H^t = e^{i\pi t/2}\begin{bmatrix} \cos(\frac{t}{2}) + \frac{i}{\sqrt{2}}\sin(\frac{t}{2})) & \frac{i}{\sqrt{2}}\sin(\frac{t}{2}) \\ \frac{i}{\sqrt{2}}\sin(\frac{t}{2}) & \cos(\frac{t}{2}) - \frac{i}{\sqrt{2}}\sin(\frac{t}{2}) \end{bmatrix} \tag{30}$$

4.6 T gates

All the of preceding discrete 1-qubit gates (Pauli gates, quarter turns, Hadamard and Hadamard-like gates) are examples of a special class of gates called Clifford gates. Although important, the Clifford gates have the notable restricting that they aren't universal – you can't build an arbitrary qubit rotation from Clifford gates alone. The is because the Clifford gates always map the x, y and z axes back onto themselves. In order to be computational universal, it is necessary to have at least one non-Clifford gate in your gate set, and the most common choice for that non-Clifford gate is the T gate, one eight of a rotation anti-clockwise about the z axis. A gate set consisting of all Cliffords and the T gate is often written as "Clifford+T".

T gate ("tee", $\pi/8$) Forth root of the Z gate, $T^4 = Z$.

$$\begin{aligned} T &= Z^{\frac{1}{4}} \\ &= \begin{bmatrix} 1 & 0 \\ 0 & e^{i\frac{\pi}{4}} \end{bmatrix} \end{aligned} \tag{31}$$

$$-\boxed{T}-$$

The T gate has sometimes been called the $\pi/8$ gate since we can extract a phase and write the T gate as

$$T = e^{i\frac{\pi}{8}\pi}\begin{bmatrix} e^{-i\frac{\pi}{8}} & 0 \\ 0 & e^{+i\frac{\pi}{8}} \end{bmatrix}$$

An eight turn anti-clockwise about the $\hat{z}$ axis.

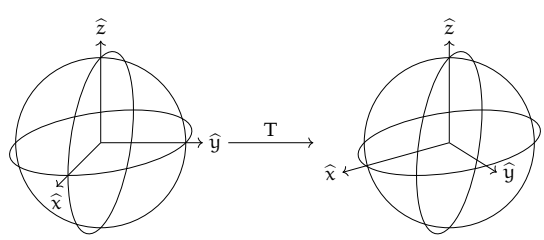

Inverse T gate Hermitian conjugate of the T gate.

$$\begin{aligned} T^\dagger &= Z^{-\frac{1}{4}} \\ &= \begin{bmatrix} 1 & 0 \\ 0 & e^{-i\frac{\pi}{4}} \end{bmatrix} \\ &\simeq R_z(\tfrac{pi}{4}) \end{aligned} \tag{32}$$

$$-\boxed{T^\dagger}-$$

An eight turn clockwise about the $\hat{z}$ axis.

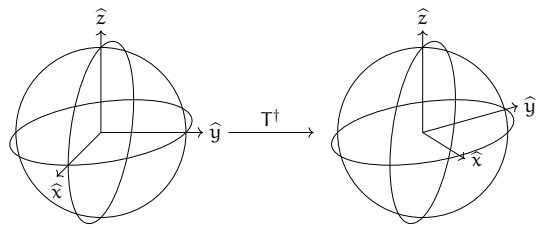

4.7 Global phase

Global phase gate (phase-shift) [15, 1, 1]

$$\begin{aligned} \mathrm{Ph}(\alpha) &= e^{i\alpha} I \\ &= \begin{bmatrix} e^{i\alpha} & 0 \\ 0 & e^{i\alpha} \end{bmatrix} \end{aligned} \tag{33}$$

$$-\boxed{\mathrm{Ph}(\alpha)}-$$

To shift the global phase we multiply the quantum state by a scalar. So it is not necessary to assign a phase shift to any particular qubit. But on those occasions where we want to keep explicit track of the phase in a circuit, it is useful to assign a global phase shift to a particular qubit and temporal location, e. g.

$$-\boxed{R_x(\theta)}- \;=\; -\boxed{\mathrm{Ph}(-\tfrac{\theta}{2})}-\boxed{X^{\frac{\theta}{\pi}}}-$$

This gate was originally called the phase-shift gate [15], but unfortunately the 1-qubit gate that shifts the phase of the 1 state relative the the zero state is also called the phase-shift gate **??**, which is potentially confusing.

Omega gate [1, 1]

$$\begin{aligned} \omega^k &= \mathrm{Ph}(\tfrac{\pi}{4}k) \\ &= \begin{bmatrix} e^{i\frac{\pi}{4}k} & 0 \\ 0 & e^{i\frac{\pi}{4}k} \end{bmatrix} \end{aligned} \tag{34}$$

An alternative parameterization of a global phase shift. This gate with integer powers crops up when constructing the 1-qubit Clifford gates from Hadamard and S gates, since $SHSHSH = \omega$. Note that $\omega^8 = I$ (**??**).

5 Decomposition of 1-qubit gates

A general 1-qubit gate corresponds to some 2 by 2 unitary matrix,

$$V = e^{i\alpha} \begin{bmatrix} a & -b^* \\ b & a^* \end{bmatrix} \tag{35}$$

where α is real, a and b are complex with $|a|^2 + |b|^2 = 1$. Given such a generic unitary, we would like to represent the gate using standard parameterized gates.

The first step to deke[3] a gate is to extract the phase factor α,

$$V = e^{i\alpha} U \tag{36}$$

so that V is a special unitary matrix with $\det V = 1$. In general, if we multiply a special unitary matrix by a complex phase c then $\det cV = c^k$ where k is the rank of the matrix, i.e. $k = 2^n$ for n qubit. (The determinate is the product of the eigenvalues, and multiplying a matrix by a constant multiplies each of the eigenvalues). [TODOO: Wordsmith]

Thus the determinate of U is $\det U = e^{i2\alpha}$, and we can extract the phase factor α with some trigonometry.

$$\alpha = \tfrac{1}{2}\text{arctan2}(\mathrm{Im}(\det U), \mathrm{Re}(\det U)) \tag{37}$$

5.1 Bloch rotation decomposition

$$R_{\vec{n}}(\theta) = \begin{bmatrix} \cos(\frac{1}{2}\theta) - in_z \sin(\frac{1}{2}\theta) & -n_y \sin(\frac{1}{2}\theta) - in_x \sin(\frac{1}{2}\theta) \\ n_y \sin(\frac{1}{2}\theta) - in_x \sin(\frac{1}{2}\theta) & \cos(\frac{1}{2}\theta) + in_z \sin(\frac{1}{2}\theta) \end{bmatrix} \tag{38}$$

$$\begin{aligned} N &= \sqrt{(\mathrm{Im}\, V_{0,1})^2 + (\mathrm{Re}\, V_{0,1})^2 + (\mathrm{Im}\, V_{0,0})^2} \\ n_x &= -\mathrm{Im}\, V_{0,1}/N \\ n_y &= -\mathrm{Re}\, V_{0,1}/N \\ n_z &= -\mathrm{Im}\, V_{0,0}/N \\ s = \sin(\tfrac{1}{2}\theta) &= -\mathrm{Im}\, V_{0,0}/n_z \\ c = \cos(\tfrac{1}{2}\theta) &= \mathrm{Re}\, V_{0,0} \\ \theta &= 2\,\text{arctan2}(s, c) \end{aligned} \tag{39}$$

5.2 Z-Y decompositions

[4]

$$U = e^{i\alpha}\, R_z(\theta_2)\, R_y(\theta_1)\, R_z(\theta_0) \tag{40}$$

Or in cirucit notation.

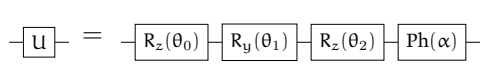

Note that we have numbered the three angles in chronological order, and recall that time runs right-to-left in operator notation, but left-to-right in circuit notation.

$$V = \begin{bmatrix} +e^{+i(+\frac{1}{2}\theta_2+\frac{1}{2}\theta_0)}\cos(\frac{1}{2}\theta_1) & -e^{-i(-\frac{1}{2}\theta_2+\frac{1}{2}\theta_0)}\sin(\frac{1}{2}\theta_1) \\ +e^{+i(+\frac{1}{2}\theta_2-\frac{1}{2}\theta_0)}\sin(\frac{1}{2}\theta_1) & +e^{-i(+\frac{1}{2}\theta_2+\frac{1}{2}\theta_0)}\cos(\frac{1}{2}\theta_1) \end{bmatrix} \tag{41}$$

The value of θ_1 can be calculated from the absolute value of either the diagonal or off-diagonal elements, provided those entries aren't close to zero. For instance, the Z-gate has zero off-diagonal entries, whereas the X-gate has zeros on the diagonal. But the diagonal and off-diagonal entries can't approach zero at the same time. So to calculate θ_1 with greatest numerical accuracy, we use whichever element has the largest absolute value.

$$\theta_1 = \begin{cases} 2\arccos(|U_{00}|), & |U_{00}| \geqslant |U_{01}| \\ 2\arcsin(|U_{01}|), & |U_{00}| < |U_{01}| \end{cases} \tag{42}$$

Having extracted θ_1, we can now calculate the sum $\theta_0 + \theta_1$ from U_{11} using the arctan2 function, (**??**),

$$\theta_0 + \theta_2 = 2\ \mathrm{arctan2}\left(\mathrm{Im}(\frac{U_{11}}{\cos(\frac{1}{2}\theta_1)}),\ \mathrm{Re}(\frac{U_{11}}{\cos(\frac{1}{2}\theta_1)})\right). \tag{43}$$

except if $\cos(\frac{1}{2}\theta_1) = 0$ then $\theta_0 + \theta_2 = 0$.

Similarly we can extract the difference $\theta_0 - \theta_2$ from U_{10}.

$$\theta_0 - \theta_2 = 2\ \mathrm{arctan2}\left(\mathrm{Im}(\frac{U_{10}}{\sin(\frac{1}{2}\theta_1)}),\ \mathrm{Re}(\frac{U_{10}}{\sin(\frac{1}{2}\theta_1)})\right) \tag{44}$$

again with an exception that if $\sin(\frac{1}{2}\theta_1) = 0$ then $\theta_0 - \theta_2 = 0$. Taking the sum and differences of (**??**) and (**??**) yields θ_0 and θ_2, which completes the decomposition.

Instead of rotation gates, we could express the same decomposition as Pauli-power gates with a simple reparameterization.

$$\begin{aligned} U =& e^{i\alpha'}\ Z^{t_2}\ Y^{t_1}\ Z^{t_0} \\ \alpha' =& \alpha + ??? \\ t_0 =& \theta_0/\pi \\ t_1 =& \theta_1/\pi \\ t_2 =& \theta_2/\pi \end{aligned} \tag{45}$$

For the IBM-??? architecture the natural 1-qubit gates are R_z and V (the square root of X) [1]. There isn't a direct access to R_y rotations or general R_x rotations, but this is only a minor restriction since $R_z(\theta) = V^\dagger R_y(\theta) V$, (Ref) and we can therefore decompose 1-qubit gates to a 5-gate sequence.

$$U = e^{i\alpha}\ R_z(\theta_2)\ V^\dagger\ R_z(\theta_1)\ V\ R_z(\theta_0) \tag{46}$$

5.3 ABC decomposition

Another useful trick is to decompose a 1-qubit unitary as $U = e^{i\alpha}AXBXC$ [15], where

$$\begin{aligned} A &= R_z(\theta_2)\, R_y(\tfrac{1}{2}\theta_1)\ , \\ B &= R_y(-\tfrac{1}{2}\theta_1)\, R_z(-\tfrac{1}{2}\theta_0 - \tfrac{1}{2}\theta_2)\ , \\ C &= R_z(\tfrac{1}{2}\theta_0 - \tfrac{1}{2}\theta_2)\ . \end{aligned}$$

Note that $ABC = I$. We will use this relation in the decomposition of 2 qubit gates .

This decomposition is the really just the Z-Y decomposition in slight disguise.

$$\begin{aligned} U &= e^{i\alpha}AXBXC \\ &= e^{i\alpha}R_z(\theta_2)\, R_y(\tfrac{1}{2}\theta_1)\, X\, R_y(-\tfrac{1}{2}\theta_1)\, X\, X\, R_z(-\tfrac{1}{2}\theta_0 - \tfrac{1}{2}\theta_2)\, X\, R_z(\tfrac{1}{2}\theta_0 - \tfrac{1}{2}\theta_2) \\ &= e^{i\alpha}R_z(\theta_2)\, R_y(\tfrac{1}{2}\theta_1) \quad R_y(+\tfrac{1}{2}\theta_1) \quad R_z(+\tfrac{1}{2}\theta_0 + \tfrac{1}{2}\theta_2) \quad R_z(\tfrac{1}{2}\theta_0 - \tfrac{1}{2}\theta_2) \\ &= e^{i\alpha}\, R_z(\theta_2)\, R_y(\theta_1) R_y(\theta_1)\, R_z(\theta_0) \end{aligned} \tag{47}$$

In the second line we insert the identity $I = XX$, and then recognize that $X\, R_z(\theta)\, X = R_x(-\theta)$ and $X\, R_y(\theta)\, X = R_y(-\theta)$. We can understand these relations by looking at the Bloch sphere. The X gate isa half turn rotation about the x axis, so the z and y axes are inverted, and the respective rotation gates induce an anti-clockwise rather than clockwise rotations relative to the original axes.

5.4 General Pauli-rotation decompositions

$$U = R_x(\theta_2)R_y(\theta_1)R_x(\theta_0) \tag{48}$$

$$V = CUC^\dagger = CR_y(\theta_2)C^\dagger\, CR_z(\theta_1)C^\dagger\, CR_y(\theta_0)C^\dagger \tag{49}$$

$$= R_z(\theta_2)R_y(\theta_1)R_z(\theta_0) \tag{50}$$

We want the single qubit gate C that moves the +Y axis to +X, but leaves the Z axis alone. This is a Clifford gate, and consulting table 3 we see that the gate is $S^\dagger$.

Table 1: Euler decompositions

Euler decomposition	Similarity transform to Z-Y-Z
X-Y-X	$h^\dagger$
X-Z-X	$R_n(+\frac{2\pi}{3}, \frac{1}{\sqrt{3}}, \frac{1}{\sqrt{3}}, \frac{1}{\sqrt{3}})$
Y-X-Y	$R_n(-\frac{2\pi}{3}, \frac{1}{\sqrt{3}}, \frac{1}{\sqrt{3}}, \frac{1}{\sqrt{3}})$
Y-Z-Y	$R_n(\pi, 0, \frac{1}{\sqrt{2}}, \frac{1}{\sqrt{2}}$
Z-X-Z	$S^\dagger$
Z-Y-Z	I

5.5 Kronecker decomposition

[17, 18]

$$C = A \otimes B \tag{51}$$

$$C_{mp;nq} = A_{mn} \otimes B_{pq} = [A_{mn} \cdot B_{pq}]^{T_{n \leftrightarrow p}} \tag{52}$$

```
import numpy as np
def nearest_kronecker_product(C):
    C = C.reshape(2, 2, 2, 2)
    C = C.transpose(0, 2, 1, 3)
    C = C.reshape(4, 4)

    u, sv, vh = np.linalg.svd(C)

    A = np.sqrt(sv[0]) * u[:, 0].reshape(2, 2)
    B = np.sqrt(sv[0]) * vh[0, :].reshape(2, 2)

    return A, B
```

We first shape C to a 4th order tensor, so that in the next line we can undo the axes transposition, before reshaping to a matrix. The singular value decomposition takes this matrix apart, and we retain the rank-1 approximation, retaining only the largest singular value and corresponding left and right singular vectors. We reshape the singular vectors to matrices to obtain our result. (multiplied by the $A \otimes B$ is the closest Kronicker product to C in the Frobenius norm.

6 The canonical gate

The canonical gate is a 3-parameter quantum logic gate that acts on two qubits [1, 1, 1].

$$\begin{aligned}&\mathsf{CAN}(t_x, t_y, t_z)\\&\quad=\exp\Big(-i\frac{\pi}{2}(t_x X\otimes X + t_y Y\otimes Y + t_z Z\otimes Z)\Big)\end{aligned} \tag{53}$$

Here, $X = \left(\begin{smallmatrix}0&1\\1&0\end{smallmatrix}\right)$, $Y = \left(\begin{smallmatrix}0&-i\\i&0\end{smallmatrix}\right)$, and $Z = \left(\begin{smallmatrix}1&0\\0&-1\end{smallmatrix}\right)$ are the 1-qubit Pauli matrices.

Note that other parameterizations are common in the literature. Often there will be a sign flip and/or the $\frac{\pi}{2}$ factor is absorbed into the parameters. The parameterization used here the nice feature that it corresponds to powers of direct products of Pauli operators (up to phase) (see (59), (63), (**??**)) .

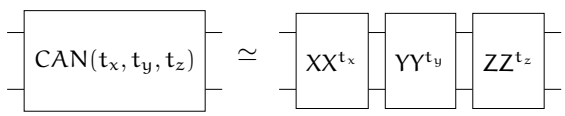

The canonical gate is, in a sense, the elementary 2-qubit gate, since any other 2-qubit gate can be decomposed into a canonical gate, and local 1-qubit interactions [19, 20, 21, 22].

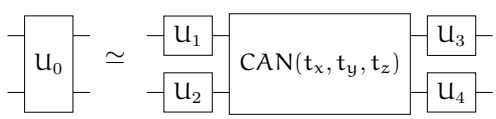

Here we use '$\simeq$' to indicate that two gates have the same unitary operator up to a global (and generally irrelevant) phase factor. We'll use '$\sim$' to indicate that two gates are locally equivalent, in that they can be mapped to one another by local 1-qubit rotations.

The canonical gate is periodic in each parameters with period 4, or period 2 if we neglect a -1 global phase factor. Thus we can constrain each parameter to the range $[-1, 1)$. Since $X\otimes X$, $Y\otimes Y$, and $Z\otimes Z$ all commute, the parameter space has the topology of a 3-torus.

However, the canonical coordinates of any given 2-qubit gate are not unique since we have considerable freedom in the prepended and appended local gates. To remove these symmetries we can constraint the canonical parameters to a "Weyl chamber" [1, 1].

$$(\tfrac{1}{2} \geqslant t_x \geqslant t_y \geqslant t_z \geqslant 0) \cup (\tfrac{1}{2} \geqslant (1-t_x) \geqslant t_y \geqslant t_z > 0) \tag{54}$$

This Weyl chamber forms a trirectangular tetrahedron. All gates in the Weyl chamber are locally inequivalent (They cannot be obtained from each other via local 1-qubit gates). The net of the Weyl chamber is illustrated in Fig. 8, and the coordinates of many common 2-qubit gates are listed in table 2. Code for performing a canonical-decomposition, and therefore of determining the Weyl coordinates, can be found in the decompositions subpackage of `QuantumFlow` [**?**].

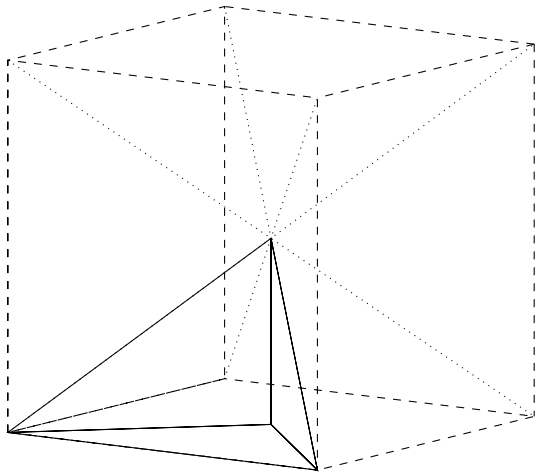

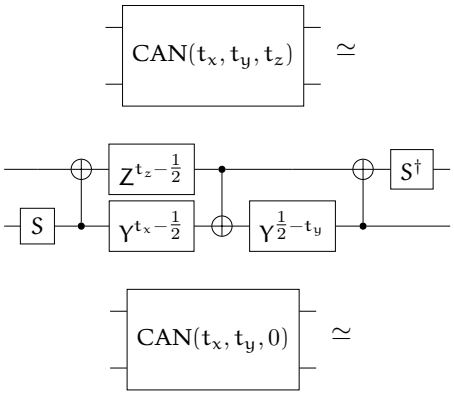
CAN(t_x, t_y, t_z)
≃
S
$Z^{t_z-\frac{1}{2}}$
$Y^{t_x-\frac{1}{2}}$
$Y^{\frac{1}{2}-t_y}$
$S^\dagger$

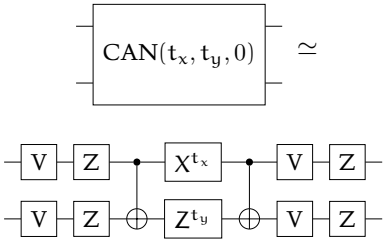
CAN($t_x, t_y, 0$)
≃
V
Z
X^{t_x}
Z^{t_y}

Table 2: Canonical coordinates of common 2-qubit gates

Gate	t_x	t_y	t_z	t'_x	t'_y	t'_z
	$\leqslant\frac{1}{2}$			$>\frac{1}{2}$		
I_2	0	0	0	1	0	0
CNOT / CZ / MS	$\frac{1}{2}$	0	0			
iSWAP / DCNOT	$\frac{1}{2}$	$\frac{1}{2}$	0	$\frac{3}{4}$	$\frac{1}{2}$	0
SWAP	$\frac{1}{2}$	$\frac{1}{2}$	$\frac{1}{2}$			
CV	$\frac{1}{4}$	0	0	$\frac{3}{4}$	0	0
$\sqrt{\text{iSWAP}}$	$\frac{1}{4}$	$\frac{1}{4}$	0	$\frac{3}{4}$	$\frac{1}{4}$	0
DB	$\frac{3}{8}$	$\frac{3}{8}$	0	$\frac{5}{8}$	$\frac{3}{8}$	0
$\sqrt{\text{SWAP}}$	$\frac{1}{4}$	$\frac{1}{4}$	$\frac{1}{4}$			
$\sqrt{\text{SWAP}}^\dagger$				$\frac{3}{4}$	$\frac{1}{4}$	$\frac{1}{4}$
B	$\frac{1}{2}$	$\frac{1}{4}$	0			
ECP	$\frac{1}{2}$	$\frac{1}{4}$	$\frac{1}{4}$			
QFT_2	$\frac{1}{2}$	$\frac{1}{2}$	$\frac{1}{4}$			
Sycamore	$\frac{1}{2}$	$\frac{1}{2}$	$\frac{1}{12}$			
Ising / CPHASE	t	0	0			
XY	t	t	0	t	1-t	0
Exchange / SWAP^α	t	t	t	t	1-t	1-t
PSWAP	$\frac{1}{2}$	$\frac{1}{2}$	t			
Special orthogonal	t_x	t_y	0			
Improper orthogonal	$\frac{1}{2}$	t_y	t_z			
XXY	t	t	δ	t	1-t	δ
	δ	t	t	δ	t	t

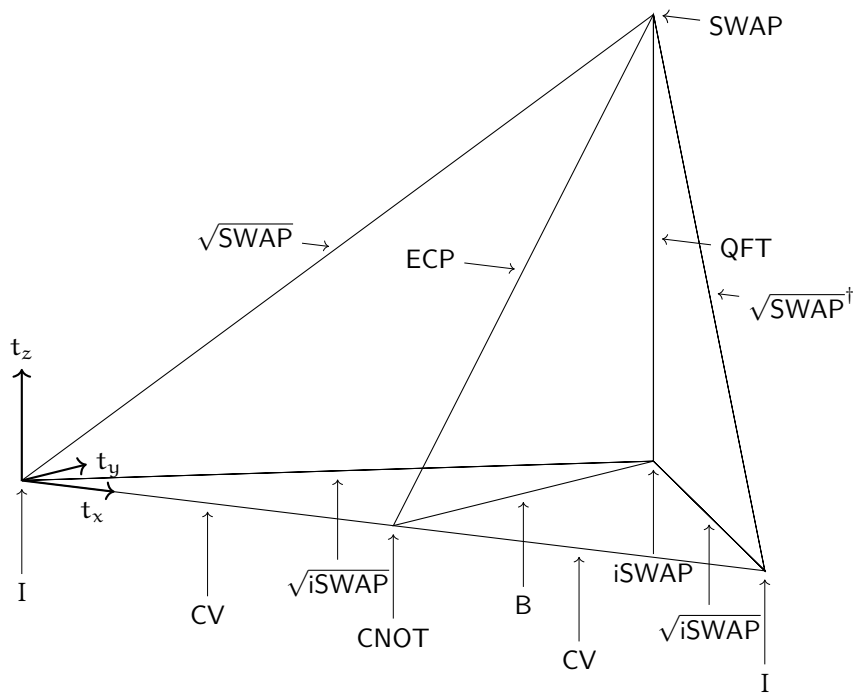

Figure 7: Location of the 11 principal 2-qubit gates in the Weyl chamber. All of these gates have coordinates of the form $\mathsf{CAN}(\frac{1}{4}k_x, \frac{1}{4}k_y, \frac{1}{4}k_z)$, for integer k_x, k_y, and k_z. Note there is a symmetry on the bottom face such that $\mathsf{CAN}(t_x, t_y, 0) \sim \mathsf{CAN}(\frac{1}{2} - t_x, t_y, 0)$.

7 Standard 2-qubit gates

7.1 Clifford gates

There are four unique 2-qubits gates in the Clifford group (up to local 1-qubit Cliffords): the identity, CNOT, iSWAP, and SWAP gates.

Identity gate

$$\begin{aligned} \mathrm{I}_2 &= \begin{pmatrix} 1&0&0&0\\0&1&0&0\\0&0&1&0\\0&0&0&1 \end{pmatrix} \\ &= \mathsf{CAN}(0,0,0) \end{aligned} \tag{55}$$

Controlled-NOT gate (CNOT, controlled-X, CX)

$$\begin{aligned} \mathsf{CNOT} &= \begin{pmatrix} 1&0&0&0\\0&1&0&0\\0&0&0&1\\0&0&1&0 \end{pmatrix} \\ &\sim \mathsf{CAN}(\tfrac{1}{2},0,0) \end{aligned} \tag{56}$$

$$\begin{aligned} \mathsf{H}_{\mathsf{CNOT}} &= \tfrac{1}{2}(\mathrm{I}-\mathsf{Z})\otimes \mathsf{H}_{\mathsf{X}} \\ &= -\tfrac{\pi}{4}(\mathrm{I}-\mathsf{Z})\otimes(\mathrm{I}-\mathsf{X}) \end{aligned}$$

Commonly represented by the circuit diagrams

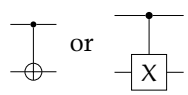

The CNOT gate is not symmetric between the two qubits. But we can switch control • and target ⊕ with local Hadamard gates.

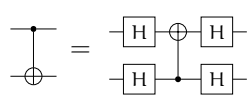

iSWAP-gate

$$\begin{aligned} \mathsf{iSWAP} &= \begin{pmatrix} 1&0&0&0\\0&0&\mathrm{i}&0\\0&\mathrm{i}&0&0\\0&0&0&1 \end{pmatrix} \\ &\simeq \mathsf{CAN}(-\tfrac{1}{2},-\tfrac{1}{2},0) \end{aligned} \tag{57}$$

SWAP-gate

$$\begin{aligned} \mathsf{SWAP} &= \begin{pmatrix} 1&0&0&0\\0&0&1&0\\0&1&0&0\\0&0&0&1 \end{pmatrix} \\ &\simeq \mathsf{CAN}(\tfrac{1}{2},\tfrac{1}{2},\tfrac{1}{2}) \end{aligned} \tag{58}$$

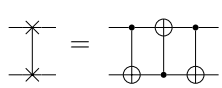

7.2 XX gates

Gates in the XX (or Ising) class have coordinates $\mathsf{CAN}(t, 0, 0)$, which forms the front edge of the Weyl chamber. This includes the identity and CNOT gates.

XX gate (Ising)

$$\begin{aligned}\mathsf{XX}(t) &= e^{-i\frac{\pi}{2}tX\otimes X} \\ &= \begin{bmatrix} \cos(\frac{\pi}{2}t) & 0 & 0 & -i\sin(\frac{\pi}{2}t) \\ 0 & \cos(\frac{\pi}{2}t) & -i\sin(\frac{\pi}{2}t) & 0 \\ 0 & -i\sin(\frac{\pi}{2}t) & \cos(\frac{\pi}{2}t) & 0 \\ -i\sin(\frac{\pi}{2}t) & 0 & 0 & \cos(\frac{\pi}{2}t) \end{bmatrix} \\ &= \mathsf{CAN}(t, 0, 0)\end{aligned} \tag{59}$$

Mølmer-Sørensen gate (MS) [23, 24]

$$\begin{aligned}\mathsf{MS} &= \frac{1}{\sqrt{2}}\begin{pmatrix} 1 & 0 & 0 & i \\ 0 & 1 & i & 0 \\ 0 & i & 1 & 0 \\ i & 0 & 0 & 1 \end{pmatrix} \\ &= \mathsf{CAN}(-\tfrac{1}{2}, 0, 0) \\ &\sim \mathsf{CAN}(\tfrac{1}{2}, 0, 0) \\ &\sim \mathsf{CNOT}\end{aligned} \tag{60}$$

Proposed as a natural gate for laser driven trapped ions. Locally equivalent to CNOT. The Mølmer-Sørensen gate, or more exactly its complex conjugate $\mathsf{MS}^\dagger = \mathsf{CAN}(\frac{1}{2}, 0, 0)$ is the natural canonical representation of the CNOT/CZ/MS gate family.

Magic gate (M) [1, 1, 1]

$$\mathsf{M} = \frac{1}{\sqrt{2}}\begin{bmatrix} 1 & i & 0 & 0 \\ 0 & 0 & i & 1 \\ 0 & 0 & i & -1 \\ 1 & -i & 0 & 0 \end{bmatrix} \tag{61}$$

$$\sim \mathsf{CAN}(\tfrac{1}{2}, 0, 0) \tag{62}$$

[25]

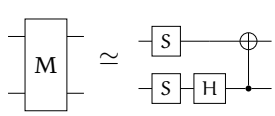

YY gate

$$\begin{aligned}
\mathsf{YY}(t) &= e^{-i\frac{\pi}{2}t\,Y\otimes Y} \\
&= \begin{pmatrix} \cos(\frac{\pi}{2}t) & 0 & 0 & +i\sin(\frac{\pi}{2}t) \\ 0 & \cos(\frac{\pi}{2}t) & -i\sin(\frac{\pi}{2}t) & 0 \\ 0 & -i\sin(\frac{\pi}{2}t) & \cos(\frac{\pi}{2}t) & 0 \\ +i\sin(\frac{\pi}{2}t) & 0 & 0 & \cos(\frac{\pi}{2}t) \end{pmatrix} \\
&= \mathsf{CAN}(0,t,0) \\
&\sim \mathsf{CAN}(t,0,0)
\end{aligned} \tag{63}$$

ZZ gate

$$\begin{aligned}
\mathsf{ZZ}(t) &= e^{-i\frac{\pi}{2}t\,Z\otimes Z} \\
&= \begin{pmatrix} 1 & 0 & 0 & 0 \\ 0 & e^{-i\pi t} & 0 & 0 \\ 0 & 0 & e^{-i\pi t} & 0 \\ 0 & 0 & 0 & 1 \end{pmatrix} \\
&= \mathsf{CAN}(0,0,t) \\
&\sim \mathsf{CAN}(t,0,0)
\end{aligned} \tag{64}$$

Controlled-Y gate

$$\begin{aligned}
\mathsf{CY} &= \begin{pmatrix} 1 & 0 & 0 & 0 \\ 0 & 1 & 0 & 0 \\ 0 & 0 & 0 & -i \\ 0 & 0 & +i & 0 \end{pmatrix} \\
&\sim \mathsf{CAN}(\tfrac{1}{2},0,0)
\end{aligned} \tag{65}$$

Commonly represented by the circuit diagram:

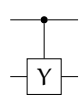

Controlled-Z gate (CZ or CSIGN)

$$\begin{aligned}
\mathsf{CZ} &= \begin{pmatrix} 1 & 0 & 0 & 0 \\ 0 & 1 & 0 & 0 \\ 0 & 0 & 1 & 0 \\ 0 & 0 & 0 & -1 \end{pmatrix} \\
&\sim \mathsf{CAN}(\tfrac{1}{2},0,0)
\end{aligned} \tag{66}$$

Commonly represented by the circuit diagrams

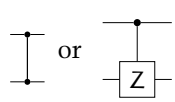

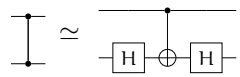

Controlled-V gate (square root of CNOT gate):

$$\begin{aligned} \mathsf{CV} &= \begin{pmatrix} 1 & 0 & 0 & 0 \\ 0 & 1 & 0 & 0 \\ 0 & 0 & \frac{1+i}{2} & \frac{1-i}{2} \\ 0 & 0 & \frac{1-i}{2} & \frac{1+i}{2} \end{pmatrix} \\ &\sim \mathsf{CAN}(\tfrac{1}{4}, 0, 0) \end{aligned} \tag{67}$$

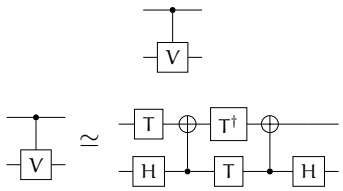

The CV gate is a square-root of CNOT, since the V-gate is the square root of the X-gate

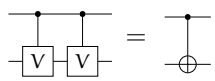

Note that the inverse $\mathsf{CV}^\dagger$ is a distinct square-root of CNOT. However CV and $\mathsf{CV}^\dagger$ are locally equivalent, which is a consequence of the symmetry about $t_x = \frac{1}{2}$ on the bottom face of the Weyl chamber.

Barenco gate :

7.3 XY gates

Gates in the XY class forms two edges of the Weyl chamber with coordinates $\mathsf{CAN}(t, t, 0)$ (for $t \leqslant \frac{1}{2}$) and $\mathsf{CAN}(t, 1-t, 0)$ (for $t > \frac{1}{2}$). This includes the identity and iSWAP gates.

XY-gate Also occasionally referred to as the piSWAP (or parametric iSWAP) gate.

$$\begin{aligned} \mathsf{XY}(t) &= \begin{pmatrix} 1 & 0 & 0 & 0 \\ 0 & \cos(\pi t) & -i\sin(\pi t) & 0 \\ 0 & -i\sin(\pi t) & \cos(\pi t) & 0 \\ 0 & 0 & 0 & 1 \end{pmatrix} \\ &= \mathsf{CAN}(t, t, 0) \\ &\sim \mathsf{CAN}(t, 1-t, 0) \end{aligned} \tag{68}$$

Double Controlled NOT gate (DCNOT)[?]

$$\begin{aligned} \mathsf{DCNOT} &= \begin{bmatrix} 1 & 0 & 0 & 0 \\ 0 & 0 & 0 & 1 \\ 0 & 1 & 0 & 0 \\ 0 & 0 & 1 & 0 \end{bmatrix} \\ &\sim \mathsf{CAN}(\tfrac{1}{2}, \tfrac{1}{2}, 0) \end{aligned} \tag{69}$$

A CNOT gate immediately followed by another CNOT with control and target interchanged. The DCNOT gate is in the iSWAP locality class.

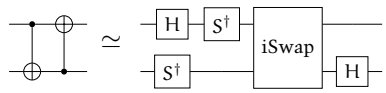

Note that unlike iSWAP, action of DCNOT is not invariant to the interchange of qubits.

Givens gate

$$\begin{aligned}\mathsf{Givens} &= \exp(-\mathrm{i}\theta(\mathsf{Y}\otimes\mathsf{X}-\mathsf{X}\otimes\mathsf{Y})/2) && (70)\\ &= \begin{bmatrix}1 & 0 & 0 & 0\\ 0 & \cos(\theta) & -\sin(\theta) & 0\\ 0 & \sin(\theta) & \cos(\theta) & 0\\ 0 & 0 & 0 & 1\end{bmatrix} && (71)\\ &\sim \mathsf{CAN}(\tfrac{1}{2},\tfrac{1}{2},0)\end{aligned}$$

bSWAP (Bell-Rabi) gate [26]

$$\begin{aligned}\mathsf{bSWAP} &= \begin{pmatrix}0 & 0 & 0 & -\mathrm{i}\\ 0 & 1 & 0 & 0\\ 0 & 0 & 1 & 0\\ -\mathrm{i} & 0 & 0 & 0\end{pmatrix}\begin{bmatrix}0 & 0 & 0 & -\mathrm{i}\\ 0 & +1 & 0 & 0\\ 0 & 0 & +1 & 0\\ -\mathrm{i} & 0 & 0 & 0\end{bmatrix} && (72)\\ &= \mathsf{CAN}(\tfrac{1}{2},-\tfrac{1}{2},0)\\ &\sim \mathsf{CAN}(\tfrac{1}{2},\tfrac{1}{2},0)\end{aligned}$$

Mystery gate

$$\begin{bmatrix}+1 & 0 & 0 & 0\\ 0 & +1 & +1 & 0\\ 0 & -1 & +1 & 0\\ 0 & 0 & 0 & +1\end{bmatrix} \sim \mathsf{Can}(\tfrac{1}{2},\tfrac{1}{2},0) \qquad (73)$$

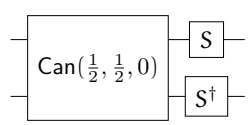

Dagwood Bumstead (DB) gate [27] Of all the gates in the XY class, the Dagwood Bumstead-gate makes the biggest sandwiches. [27, Fig. 4]

$$\begin{aligned}\mathsf{DB} &= \begin{bmatrix}1 & 0 & 0 & 0\\ 0 & \cos(\frac{3\pi}{8}) & -\mathrm{i}\sin(\frac{3\pi}{8}) & 0\\ 0 & -\sin(\frac{3\pi}{8}) & \cos(\frac{3\pi}{8}) & 0\\ 0 & 0 & 0 & 1\end{bmatrix} && (74)\\ &= \mathsf{XY}(\tfrac{3}{8})\\ &= \mathsf{CAN}(\tfrac{3}{8},\tfrac{3}{8},0)\end{aligned}$$

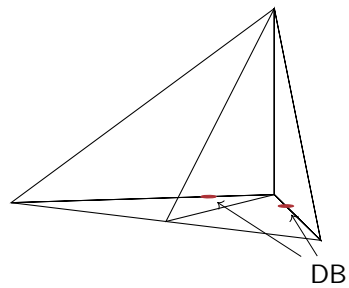

7.4 Exchange-interaction gates

Includes the identity and SWAP gates.

EXCH (XXX) gate

$$\mathsf{EXCH}(t) = \mathsf{CAN}(t, t, t) \tag{75}$$

SWAP-alpha gates

$$\mathsf{SWAP}^{\alpha} \sim \mathsf{CAN}(\alpha, \alpha, \alpha) \tag{76}$$

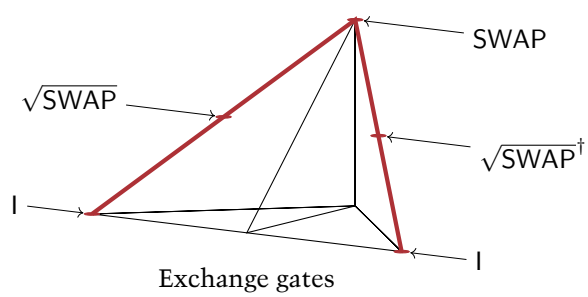

Exchange gates

$\sqrt{\mathsf{SWAP}}$-gate

$$\sqrt{\mathsf{SWAP}} = \begin{pmatrix} 1 & 0 & 0 & 0 \\ 0 & \frac{1}{2}(1+i) & \frac{1}{2}(1-i) & 0 \\ 0 & \frac{1}{2}(1-i) & \frac{1}{2}(1+i) & 0 \\ 0 & 0 & 0 & 1 \end{pmatrix} = \mathsf{CAN}(\tfrac{1}{4}, \tfrac{1}{4}, \tfrac{1}{4}) \tag{77}$$

Inverse $\sqrt{\mathsf{SWAP}}$-gate

$$\sqrt{\mathsf{SWAP}}^{\dagger} = \begin{pmatrix} 1 & 0 & 0 & 0 \\ 0 & \frac{1}{2}(1-i) & \frac{1}{2}(1+i) & 0 \\ 0 & \frac{1}{2}(1+i) & \frac{1}{2}(1-i) & 0 \\ 0 & 0 & 0 & 1 \end{pmatrix} = \mathsf{CAN}(\tfrac{3}{4}, \tfrac{1}{4}, \tfrac{1}{4}) \tag{78}$$

Because of the symmetry around $t_x = \frac{1}{2}$ on the base of the Weyl chamber, the CNOT and iSWAP gates only have one square root. But the SWAP has two locally distinct square roots, which are inverses of each other.

7.5 Parametric SWAP gates

The class of parametric SWAP (PSWAP) gates forms the back edge of the Weyl chamber, $\mathsf{CAN}(\frac{1}{2}, \frac{1}{2}, t_z)$, connecting the SWAP and iSWAP gates. These gates can be decomposed into a SWAP and ZZ gate.

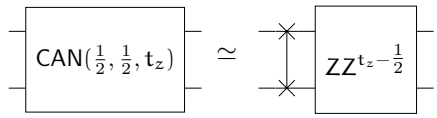

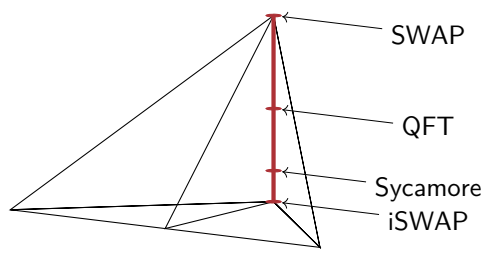

pSWAP gates

The Sycamore gate is discussed under XXY gates [ref].

pSwap gate (parametric swap) [28] The parametric swap gate as originally defined in the QUIL quantum programming language.

$$\mathsf{pSWAP}(\theta) = \begin{pmatrix} 1 & 0 & 0 & 0 \\ 0 & 0 & e^{i\theta} & 0 \\ 0 & e^{i\theta} & 0 & 0 \\ 0 & 0 & 0 & 1 \end{pmatrix} \sim \mathsf{CAN}(\tfrac{1}{2}, \tfrac{1}{2}, \tfrac{1}{2} - \tfrac{\theta}{\pi}) \tag{79}$$

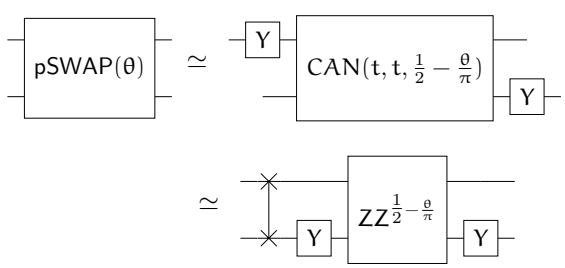

Quantum Fourier transform (QFT) [1] We will discuss the quantum Fourier transform (QFT) latter [ref]. The QFT can be applied to any number of qubits. For 2-qubits, the QFT gate is in the PSWAP class, half way between SWAP and iSWAP.

$$\mathsf{QFT}_2 = \frac{1}{2}\begin{bmatrix} 1 & 1 & 1 & 1 \\ 1 & i & -1 & -i \\ 1 & -1 & 1 & -1 \\ 1 & -i & -1 & i \end{bmatrix} \sim \mathsf{CAN}(\tfrac{1}{2}, \tfrac{1}{2}, \tfrac{1}{4}) \tag{80}$$

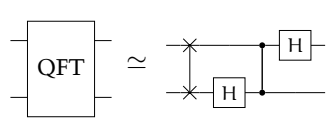

7.6 Orthogonal gates

An orthogonal gate, in this context, is a gate that can be represented by an orthogonal matrix (up to local 1-qubit rotations.) The special orthogonal gates have determinant $+1$ and coordinates $\mathsf{CAN}(t_x, t_y, 0)$, which covers the bottom surface of the canonical Weyl chamber.

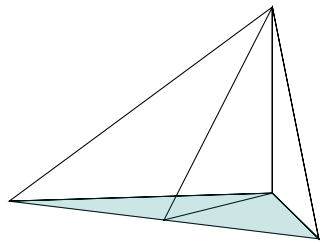

Special orthogonal gates

The improper orthogonal gates have determinant -1 and coordinates $\mathsf{CAN}(\frac{1}{2}, t_y, t_z)$, which is a plane connecting the CNOT, iSWAP, and SWAP gates.

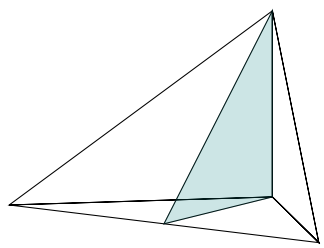

Improper orthogonal gates

B (Berkeley) gate [29] Located in the middle of the bottom face of the Weyl chamber.

$$\begin{aligned}
\mathsf{B} &= \begin{pmatrix} \cos(\frac{\pi}{8}) & 0 & 0 & i\sin(\frac{\pi}{8}) \\ 0 & \cos(\frac{3\pi}{8}) & i\sin(\frac{3\pi}{8}) & 0 \\ 0 & i\sin(\frac{3\pi}{8}) & \cos(\frac{3\pi}{8}) & 0 \\ i\sin(\frac{\pi}{8}) & 0 & 0 & \cos(\frac{\pi}{8}) \end{pmatrix} \\
&= \frac{\sqrt{2-\sqrt{2}}}{2} \begin{pmatrix} 1+\sqrt{2} & 0 & 0 & i \\ 0 & 1 & i(1+\sqrt{2}) & 0 \\ 0 & i(1+\sqrt{2}) & 1 & 0 \\ i & 0 & 0 & 1+\sqrt{2} \end{pmatrix} \\
&= \mathsf{CAN}(-\tfrac{1}{2}, -\tfrac{1}{4}, 0)
\end{aligned} \tag{81}$$

The B-gate, as originally defined, has canonical parameters outside our Weyl chamber due to differing conventions for parameterization of the canonical gate. But of course it can be moved into our Weyl chamber with local gates.

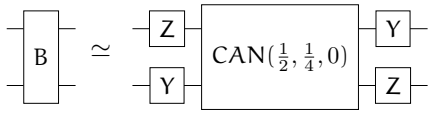

The B-gate is half way between the CNOT and DCNOT (~ iSWAP) gates,

and thus it can be constructed from 3 CV (square root of CNOT) gates.

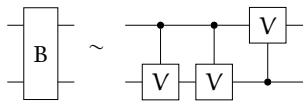

Notably two-B gates are sufficient to create any other 2-qubit gate (whereas, for example, we need 3 CNOT's in general) [29] [5]

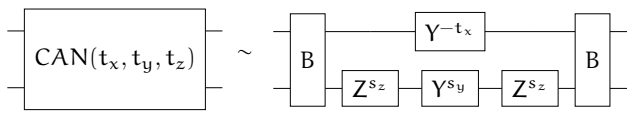

$$
\begin{aligned}
s_y &= +\tfrac{1}{\pi}\arccos\left(1-4\sin^2\tfrac{1}{2}\pi t_y\cos^2\tfrac{1}{2}\pi t_z\right)\\
s_z &= -\tfrac{1}{\pi}\arcsin\sqrt{\frac{\cos\pi t_y\cos\pi t_z}{1-2\sin^2\tfrac{1}{2}\pi t_y\cos^2\tfrac{1}{2}\pi t_z}}
\end{aligned}
\tag{82}
$$

ECP-gate [27]

$$
\begin{aligned}
\mathsf{ECP} &= \frac{1}{2}\begin{pmatrix} 2c & 0 & 0 & -i2s\\ 0 & (1+i)(c-s) & (1-i)(c+s) & 0\\ 0 & (1-i)(c+s) & (1+i)(c-s) & 0\\ -i2s & 0 & 0 & 2c\end{pmatrix}\\
c &= \cos(\tfrac{\pi}{8}) = \sqrt{\tfrac{2+\sqrt{2}}{2}}\\
s &= \sin(\tfrac{\pi}{8}) = \sqrt{\tfrac{2-\sqrt{2}}{2}}\\
&= \mathsf{CAN}(\tfrac{1}{2},\tfrac{1}{4},\tfrac{1}{4})
\end{aligned}
\tag{83}
$$

The peak of the pyramid of gates in the Weyl chamber that can be created with a square-root of iSWAP sandwich. Equivalent to $\mathsf{Can}(\frac{1}{2},\frac{1}{4},\frac{1}{4})$.

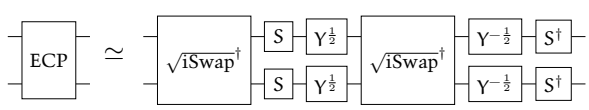

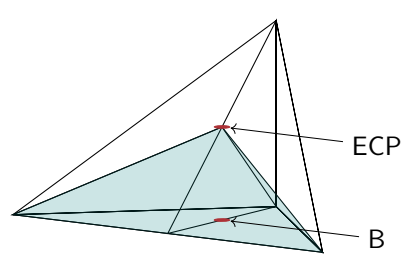

B and ECP gates, and ECP pyramid

W-gate [1] A 2-qubit orthogonal and Hermitian gate (and therefore also symmetric) $W^\dagger = W$, that applies a Hadamard gate to a duel-rail encoded

qubit.

$$\mathsf{W} = \begin{bmatrix} 1 & 0 & 0 & 0 \\ 0 & \frac{1}{\sqrt{2}} & \frac{1}{\sqrt{2}} & 0 \\ 0 & \frac{1}{\sqrt{2}} & -\frac{1}{\sqrt{2}} & 0 \\ 0 & 0 & 0 & 1 \end{bmatrix} \sim \mathsf{ECP} = \mathsf{CAN}(\tfrac{1}{2}, \tfrac{1}{4}, \tfrac{1}{4}) \tag{84}$$

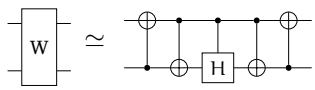

This W gate is locally equivalent to ECP,

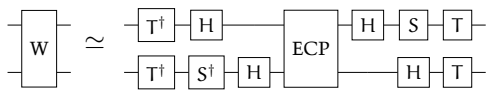

and thus three CNOT gates are necessary (and sufficient) to generate the gate.

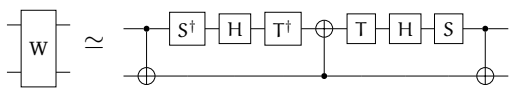

The W gate has the useful property that it diagonlizes the swap gate [1].

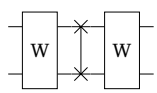

$$= \begin{bmatrix} 1 & 0 & 0 & 0 \\ 0 & 1 & 0 & 0 \\ 0 & 0 & -1 & 0 \\ 0 & 0 & 0 & 1 \end{bmatrix}$$

7.7 XXY gates

The remaining faces of the Weyl chamber are the XXY family. Thanks to the Weyl symmetries, this family covers all three faces that meet at the SWAP gate.

$$\mathsf{XXY}(t, \delta) = \mathsf{CAN}(t, t, \delta) \tag{85}$$

FSIM (Ferminoic Simulator) gate [1]

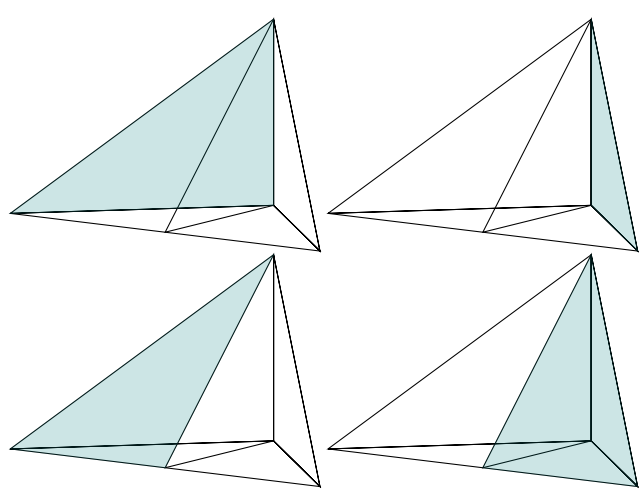

Sycamore **gate** [1]

8 Standard 3-qubit gates

Toffoli gate (controlled-controlled-not, CCNOT) [30, 15]

$$\mathrm{CCNOT} = \begin{bmatrix} 1&0&0&0&0&0&0&0\\ 0&1&0&0&0&0&0&0\\ 0&0&1&0&0&0&0&0\\ 0&0&0&1&0&0&0&0\\ 0&0&0&0&1&0&0&0\\ 0&0&0&0&0&1&0&0\\ 0&0&0&0&0&0&0&1\\ 0&0&0&0&0&0&1&0 \end{bmatrix} \tag{86}$$

$$\begin{aligned} H_{\mathrm{CCNOT}} &= -\tfrac{\pi}{8}(I_0 - Z_0)(I_1 - Z_1)(I_2 - X_2) \\ &= \tfrac{\pi}{2}\begin{bmatrix} 0&0&0&0&0&0&0&0\\ 0&0&0&0&0&0&0&0\\ 0&0&0&0&0&0&0&0\\ 0&0&0&0&0&0&0&0\\ 0&0&0&0&0&0&0&0\\ 0&0&0&0&0&0&0&0\\ 0&0&0&0&0&0&-1&1\\ 0&0&0&0&0&0&1&-1 \end{bmatrix} \end{aligned} \tag{87}$$

Fredkin gate (controlled-swap, CSWAP) [31, 1]

$$\mathrm{CSWAP} = \begin{bmatrix} 1&0&0&0&0&0&0&0\\ 0&1&0&0&0&0&0&0\\ 0&0&1&0&0&0&0&0\\ 0&0&0&1&0&0&0&0\\ 0&0&0&0&1&0&0&0\\ 0&0&0&0&0&0&1&0\\ 0&0&0&0&0&1&0&0\\ 0&0&0&0&0&0&0&1 \end{bmatrix} \tag{88}$$

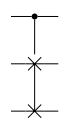

$$\begin{aligned} H_{\mathrm{CSWAP}} &= -\tfrac{\pi}{8}(I_0 - Z_0)(X_1X_2 + Y_1Y_2 + Z_1Z_2 - I_1I_2) \\ &= \tfrac{\pi}{2}\begin{bmatrix} 0&0&0&0&0&0&0&0\\ 0&0&0&0&0&0&0&0\\ 0&0&0&0&0&0&0&0\\ 0&0&0&0&0&0&0&0\\ 0&0&0&0&0&0&0&0\\ 0&0&0&0&0&-1&1&0\\ 0&0&0&0&0&1&-1&0\\ 0&0&0&0&0&0&0&0 \end{bmatrix} \end{aligned} \tag{89}$$

CCZ gate (controlled-controlled-Z)

$$\mathrm{CCZ} = \begin{bmatrix} 1&0&0&0&0&0&0&0\\ 0&1&0&0&0&0&0&0\\ 0&0&1&0&0&0&0&0\\ 0&0&0&1&0&0&0&0\\ 0&0&0&0&1&0&0&0\\ 0&0&0&0&0&1&0&0\\ 0&0&0&0&0&0&1&0\\ 0&0&0&0&0&0&0&-1 \end{bmatrix} \tag{90}$$

Peres gate [32]

$$\text{Peres} = \begin{bmatrix} 1&0&0&0&0&0&0&0 \\ 0&1&0&0&0&0&0&0 \\ 0&0&1&0&0&0&0&0 \\ 0&0&0&1&0&0&0&0 \\ 0&0&0&0&0&0&0&1 \\ 0&0&0&0&0&0&1&0 \\ 0&0&0&0&0&1&0&0 \\ 0&0&0&0&1&0&0&0 \end{bmatrix} \tag{91}$$

Another gate that is universal for classical reversible computing. It is equivalent to a Toffoli followed by a CNOT gate.

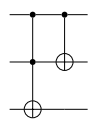

Deutsch gate [33, 34, 35] Mostly of historical interest, since this was the first quantum gate to be shown to be computationally universal [33].

$$\text{Deutsch}(\theta) = \begin{bmatrix} 1&0&0&0&0&0 & 0 & 0 \\ 0&1&0&0&0&0 & 0 & 0 \\ 0&0&1&0&0&0 & 0 & 0 \\ 0&0&0&1&0&0 & 0 & 0 \\ 0&0&0&0&1&0 & 0 & 0 \\ 0&0&0&0&0&1 & 0 & 0 \\ 0&0&0&0&0&0 & i\cos(\theta) & \sin(\theta) \\ 0&0&0&0&0&0 & \sin(\theta) & i\cos(\theta) \end{bmatrix} \tag{92}$$

Examining the controlled unitary sub-matrix, the Deutsch gate can be thought of as a controlled-controlled-$iR_x(\theta)^2$ gate. gate.

$\text{Deutsch}(\theta) =$

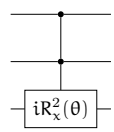

Barenco [34] demonstrated a construction of the Deutsch gate from 2-qubit "Barenco" gates, demonstrating that 2-qubits gates are sufficient for universality.

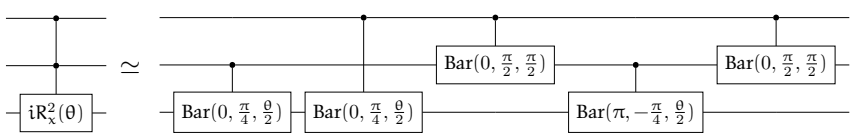

9 2-Level Unitary gates

A 2-level unitary is a unitary operation that acts non-trivially on only 2-states. For 2-qubits, any controlled-unitary gate is 2-level,

$$\begin{bmatrix} 1 & 0 & 0 & 0 \\ 0 & 1 & 0 & 0 \\ 0 & 0 & a & c \\ 0 & 0 & b & d \end{bmatrix} \tag{93}$$

where the 2x2 submatrix $\left[\begin{smallmatrix} a & c \\ b & d \end{smallmatrix}\right]$ is unitary. But the active states need not be the last two. Any permutation of a controlled 1-qubit gate is also a two-level unitary, such as

$$\begin{bmatrix} a & c & 0 & 0 \\ b & d & 0 & 0 \\ 0 & 0 & 1 & 0 \\ 0 & 0 & 0 & 1 \end{bmatrix} \text{or} \begin{bmatrix} a & 0 & 0 & c \\ 0 & 1 & 0 & 0 \\ 0 & 0 & 1 & 0 \\ b & 0 & 0 & d \end{bmatrix}. \tag{94}$$

Similarly any multi-controlled 2x2 unitary, or permutation of the same, is a 2-level unitary.

Two-level unitaries are important because we can systematically decompose an arbitrary unitary into a sequence of 2-level unitaries, and 2-level unitaries themselves can be decomposed into controlled-unitary gates.

9.1 Two-level unitary decomposition

A d-dimensional unitary operator can be decomposed into a product of, at most, $\frac{1}{2}d(d-1)$ 2-level unitaries [? 1, 1].

We'll use a 2-qubit gate A as illustration, with dimension $d = 2^2 = 4$.

$$A = \begin{bmatrix} a_{00} & a_{01} & a_{02} & a_{03} \\ a_{10} & a_{11} & a_{12} & a_{13} \\ a_{20} & a_{21} & a_{22} & a_{23} \\ a_{30} & a_{31} & a_{32} & a_{33} \end{bmatrix} \tag{95}$$

The trick is that we can set any off-diagonal entry to zero by multiply by a carefully constructed 2-level unitary. Lets start with the $(1,0)$ entry.

$$B = U_{10}A = \begin{bmatrix} 1 & b_{01} & b_{02} & b_{03} \\ 0 & b_{11} & b_{12} & b_{13} \\ b_{20} & b_{21} & b_{22} & b_{23} \\ b_{30} & b_{31} & b_{32} & b_{33} \end{bmatrix} \quad U_{10} = \begin{bmatrix} \frac{a_{00}^*}{w} & \frac{a_{10}^*}{w} & 0 & 0 \\ \frac{a_{10}}{w} & \frac{-a_{00}}{w} & 0 & 0 \\ 0 & 0 & 1 & 0 \\ 0 & 0 & 0 & 1 \end{bmatrix} \quad w = \sqrt{|a_{00}| + |a_{10}|}$$

Following through the matrix multiplication, we see that $b_{10} = (a_{10}a_{00} - a_{00}a_{10})/w = 0$, and $b_{00} = (a_{00}^* a_{00} - a_{10}^* a_{10})/w = w/w = 1$

We can now set $(2,0)$ to zero using the same procedure,

$$C = U_{20}B = \begin{bmatrix} 1 & c_{01} & c_{02} & c_{03} \\ 0 & c_{11} & c_{12} & c_{13} \\ 0 & c_{21} & c_{22} & c_{23} \\ c_{30} & c_{31} & c_{32} & c_{33} \end{bmatrix} \quad U_{20} = \begin{bmatrix} \frac{b_{00}^*}{w} & 0 & \frac{b_{20}^*}{w} & 0 \\ 0 & 1 & 0 & 0 \\ \frac{b_{20}}{w} & 0 & \frac{-b_{00}}{w} & 0 \\ 0 & 0 & 0 & 1 \end{bmatrix} \quad w = \sqrt{|b_{00}| + |b_{20}|}$$

and then set $(3,0)$ to zero.

$$D = U_{30}C = \begin{bmatrix} 1 & 0 & 0 & 0 \\ 0 & d_{11} & d_{12} & d_{13} \\ 0 & d_{21} & d_{22} & d_{23} \\ 0 & d_{31} & d_{32} & d_{33} \end{bmatrix} \quad U_{30} = \begin{bmatrix} \frac{c_{00}^*}{w} & 0 & 0 & \frac{c_{20}^*}{w} \\ 0 & 1 & 0 & 0 \\ 0 & 0 & 1 & 0 \\ \frac{c_{20}}{w} & 0 & 0 & \frac{-c_{00}}{w} \end{bmatrix} \quad w = \sqrt{|c_{00}| + |c_{20}|}$$

Once we have set all the off diagonal elements of the left column to zero, then the off-diagonal elements of the top row must also be zero because ...

Once we repeat this procedure $\frac{1}{2}d(d-1)$ times, setting all the lower off-diagonal entries to zero, we are left with the identity matrix.

$$I = U_{32}U_{31}U_{21}U_{30}U_{20}U_{10}A \tag{96}$$

Inverting this circuit, we obtain the original unitary as a product of 2-level unitaries.

$$A = U_{10}^{\dagger}U_{20}^{\dagger}U_{30}^{\dagger}U_{21}^{\dagger}U_{31}^{\dagger}U_{32}^{\dagger} \tag{97}$$

9.2 Control-gate decomposition of 2-level unitary

10 Clifford Gates

The Clifford gates are an important subgroup of quantum gates. Familiar examples include the Pauli gates (I, X, Y, Z), phase (S), Hadamard (H), controlled-Z (CZ), controlled-not (CNOT), and swap. Common non-Clifford gates include T, B, and Toffolli (CCNOT).

The *Clifford group* C_n of gates acting on n qubits consists of those gates that *normalize* the corresponding Pauli group P_n. In the context of groups, *normalize* means that if p is an element of the Pauli group, and V is a Clifford gate, then $p' = VpV^\dagger$ is also an element of the Pauli group.

$$\mathbf{C}_n = \{V \in U_{2^n} \mid V\mathbf{P}_n V^\dagger = \mathbf{P}_n\} \tag{98}$$

The Clifford gates are defined this way because of important applications in quantum error correcting, which we will come to presently. An alternative approach is to define the Clifford group as all gates that can be constructed from S, H, and CNOT. This is the same group, up to phase.

10.1 Single qubit Clifford gates

Consider the X gate as a Clifford acting on the X, Y, and Z single-qubit Pauli elements.

$$\begin{aligned}
XXX^\dagger &= \left[\begin{smallmatrix} 0 & 1 \\ 1 & 0 \end{smallmatrix}\right]\left[\begin{smallmatrix} 0 & 1 \\ 1 & 0 \end{smallmatrix}\right]\left[\begin{smallmatrix} 0 & 1 \\ 1 & 0 \end{smallmatrix}\right] = \left[\begin{smallmatrix} 0 & 1 \\ 1 & 0 \end{smallmatrix}\right] = +X \\
XYX^\dagger &= \left[\begin{smallmatrix} 0 & 1 \\ 1 & 0 \end{smallmatrix}\right]\left[\begin{smallmatrix} 0 & -i \\ i & 0 \end{smallmatrix}\right]\left[\begin{smallmatrix} 0 & 1 \\ 1 & 0 \end{smallmatrix}\right] = \left[\begin{smallmatrix} 1 & 0 \\ 0 & -1 \end{smallmatrix}\right] = -Z \\
XZX^\dagger &= \left[\begin{smallmatrix} 0 & 1 \\ 1 & 0 \end{smallmatrix}\right]\left[\begin{smallmatrix} 1 & 0 \\ 0 & -1 \end{smallmatrix}\right]\left[\begin{smallmatrix} 0 & 1 \\ 1 & 0 \end{smallmatrix}\right] = \left[\begin{smallmatrix} 0 & -i \\ i & 0 \end{smallmatrix}\right] = -Y
\end{aligned}$$

Or the Hadamard gate

$$\begin{aligned}
HXH^\dagger &= \tfrac{1}{2}\left[\begin{smallmatrix} 1 & -1 \\ 1 & 1 \end{smallmatrix}\right]\left[\begin{smallmatrix} 0 & 1 \\ 1 & 0 \end{smallmatrix}\right]\left[\begin{smallmatrix} 1 & -1 \\ 1 & 1 \end{smallmatrix}\right] = \left[\begin{smallmatrix} 1 & 0 \\ 0 & -1 \end{smallmatrix}\right] = +Z \\
HYH^\dagger &= \tfrac{1}{2}\left[\begin{smallmatrix} 1 & -1 \\ 1 & 1 \end{smallmatrix}\right]\left[\begin{smallmatrix} 0 & -i \\ i & 0 \end{smallmatrix}\right]\left[\begin{smallmatrix} 1 & -1 \\ 1 & 1 \end{smallmatrix}\right] = \left[\begin{smallmatrix} 0 & i \\ -i & 0 \end{smallmatrix}\right] = -Y \\
HZH^\dagger &= \tfrac{1}{2}\left[\begin{smallmatrix} 1 & -1 \\ 1 & 1 \end{smallmatrix}\right]\left[\begin{smallmatrix} 1 & 0 \\ 0 & -1 \end{smallmatrix}\right]\left[\begin{smallmatrix} 1 & -1 \\ 1 & 1 \end{smallmatrix}\right] = \left[\begin{smallmatrix} 0 & 1 \\ 1 & 0 \end{smallmatrix}\right] = +X
\end{aligned}$$

Note that we only ever pick up a ± 1 phase, and never an imaginary phase. This is because any element of the Pauli group with ± 1 phase is Hermitian, and the transformed gate $UpU^\dagger$ must also Hermitian. Therefore we can't pick up an imaginary phase.

On the other hand, if we look at these transformations for a non-Clifford gate such as the T gate, we do not recover Pauli elements.

$$\begin{aligned}
TXT^\dagger &= \left[\begin{smallmatrix} 1 & 0 \\ 0 & e^{+i\frac{\pi}{4}} \end{smallmatrix}\right]\left[\begin{smallmatrix} 0 & 1 \\ 1 & 0 \end{smallmatrix}\right]\left[\begin{smallmatrix} 1 & 0 \\ 0 & e^{-i\frac{\pi}{4}} \end{smallmatrix}\right] = \left[\begin{smallmatrix} 0 & e^{+i\frac{\pi}{4}} \\ e^{-i\frac{\pi}{4}} & 0 \end{smallmatrix}\right] \\
TYT^\dagger &= \left[\begin{smallmatrix} 1 & 0 \\ 0 & e^{+i\frac{\pi}{4}} \end{smallmatrix}\right]\left[\begin{smallmatrix} 0 & -i \\ i & 0 \end{smallmatrix}\right]\left[\begin{smallmatrix} 1 & 0 \\ 0 & e^{-i\frac{\pi}{4}} \end{smallmatrix}\right] = -\left[\begin{smallmatrix} 0 & e^{+i\frac{\pi}{4}} \\ e^{-i\frac{\pi}{4}} & 0 \end{smallmatrix}\right] \\
TZT^\dagger &= \left[\begin{smallmatrix} 1 & 0 \\ 0 & e^{+i\frac{\pi}{4}} \end{smallmatrix}\right]\left[\begin{smallmatrix} 1 & 0 \\ 0 & -1 \end{smallmatrix}\right]\left[\begin{smallmatrix} 1 & 0 \\ 0 & e^{-i\frac{\pi}{4}} \end{smallmatrix}\right] = \left[\begin{smallmatrix} 1 & 0 \\ 0 & -1 \end{smallmatrix}\right] = Z
\end{aligned}$$

Up to phase, a Clifford gate is completely determined by its transformation of the Pauli elements [TODO: Why?]. And because the Pauli group elements are tensor products acting independently on separate qubits, we need only consider the action of the Clifford group on each of the $4n$ single qubit Pauli gates. Moreover, the action of the identity is trivial, and the ac-

tion on Y can be determined by that on X and Y, since $VYV^\dagger = -iVXZV^\dagger = -i\ VXV^\dagger\ VZV^\dagger$. For single qubit Cliffords, X can map to 6 possibilities, $\{\pm X, \pm Y, \pm Z\}$, leaving 4 possibilities for the action on Z. This gives a total of $6 \times 4 = 24$ distinct 1-qubit Clifford groups.

The 24 1-qubit Clifford gates are isomorphic to the group of rotations of an octahedron. The coordinates $R_n(\theta)$ of these are listed in table ???, along with the Pauli mappings. If we think of the Pauli gates X, Y, Z as the 3 cartesian axes x, y, z, then the elements of the Clifford group correspond to rotations that map axes to axes. We have 3 elements that rotate 180° about vertices (X, Y, Z); 6 elements (the square roots of X, Y, and Z) that rotate 90° or 270° degrees around vertices; 6 Hadamard like gates that rotate 180° about edges; another 8 gates that rotation 120° or 240° degrees around faces; and the identity. This is a subgroup of the full octahedral group (which includes inversions), and also equal(??) to S_4, the group of permutations of 4 objects.

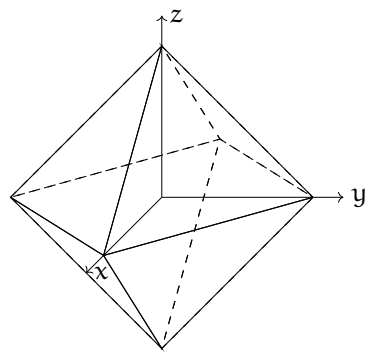

All 24 single qubit Clifford gates can be generated from just 2 elements, traditionally chosen to be S and H. For instance $X = HSSH$. Since $(SH)^3 = e^{2\pi i/8}I$ we can generate each Clifford gate with 8 different phases. This is why you'll sometimes see the number of 1-qubit Clifford gates reported as $8 \times 24 = 192$, which includes in the possible Clifford gates integers powers of a phase $\omega^k = e^{2\pi ik/8}$, $k = 0, 1, \ldots, 7$.

10.2 Two qubit Clifford gates

Lets now consider the action of the 2-qubit CNOT gate on the X and Z single-qubit Pauli elements. Recall that CNOT is its own inverse. We can commute an X gate past the CNOT target, and a Z past the CNOT control, which leads to 2 trivial cases. But the other 2 cases are more interesting. An X gate acting on the control qubit becomes a pair of X gates, and a Z on the target qubit becomes a pair of Z gates.

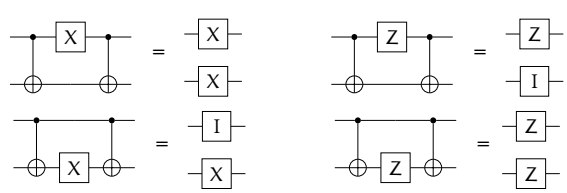

For a CZ gate, the action on Z gates is trivial, but the action on X generates an extra Z gate.

Table 3: Coordinates of the 24 1-qubit Clifford gates.

Gate	θ	n_x	n_y	n_z	X	Y	Z
I	0				+X	+Y	+Z
V	$\frac{1}{2}\pi$	1	0	0	+X	?Z	+Y
X	π	1	0	0	+X	−Y	−Z
$V^\dagger$	$-\frac{1}{2}\pi$	1	0	0			
$h^\dagger$	$\frac{1}{2}\pi$	0	1	0			
Y	π	0	1	0			
h	$-\frac{1}{2}\pi$	0	1	0			
S	$\frac{1}{2}\pi$	0	0	1			
Z	π	0	0	1			
$S^\dagger$	$-\frac{1}{2}\pi$	0	0	1			
	π	$\frac{1}{\sqrt{2}}$	$\frac{1}{\sqrt{2}}$	0			
H	π	$\frac{1}{\sqrt{2}}$	0	$\frac{1}{\sqrt{2}}$			
	π	0	$\frac{1}{\sqrt{2}}$	$\frac{1}{\sqrt{2}}$			
	π	$-\frac{1}{\sqrt{2}}$	$\frac{1}{\sqrt{2}}$	0			
	π	$\frac{1}{\sqrt{2}}$	0	$-\frac{1}{\sqrt{2}}$			
	π	0	$-\frac{1}{\sqrt{2}}$	$\frac{1}{\sqrt{2}}$			
	$\frac{2}{3}\pi$	$\frac{1}{\sqrt{3}}$	$\frac{1}{\sqrt{3}}$	$\frac{1}{\sqrt{3}}$			
	$-\frac{2}{3}\pi$	$\frac{1}{\sqrt{3}}$	$\frac{1}{\sqrt{3}}$	$\frac{1}{\sqrt{3}}$			
	$\frac{2}{3}\pi$	$-\frac{1}{\sqrt{3}}$	$\frac{1}{\sqrt{3}}$	$\frac{1}{\sqrt{3}}$			
	$-\frac{2}{3}\pi$	$-\frac{1}{\sqrt{3}}$	$\frac{1}{\sqrt{3}}$	$\frac{1}{\sqrt{3}}$			
	$\frac{2}{3}\pi$	$\frac{1}{\sqrt{3}}$	$-\frac{1}{\sqrt{3}}$	$\frac{1}{\sqrt{3}}$			
	$-\frac{2}{3}\pi$	$\frac{1}{\sqrt{3}}$	$-\frac{1}{\sqrt{3}}$	$\frac{1}{\sqrt{3}}$			
	$\frac{2}{3}\pi$	$\frac{1}{\sqrt{3}}$	$\frac{1}{\sqrt{3}}$	$-\frac{1}{\sqrt{3}}$			
	$-\frac{2}{3}\pi$	$\frac{1}{\sqrt{3}}$	$\frac{1}{\sqrt{3}}$	$-\frac{1}{\sqrt{3}}$			

Table 4: Clifford tableaus for 2-qubit gates

Gate	qubit	X	Z	Gate	qubit	X	Z
I	0	$+X \otimes I$	$+Z \otimes I$				
	1	$+I \otimes X$	$+I \otimes Z$				
CNOT	0	$+X \otimes X$	$+Z \otimes I$	CZ	0	$+X \otimes Z$	$+Z \otimes I$
	1	$+I \otimes X$	$+Z \otimes Z$		1	$+Z \otimes X$	$+I \otimes Z$
iSWAP	0	$-Z \otimes Y$	$+I \otimes Z$	DCNOT	0	$+X \otimes X$	$+I \otimes Z$
	1	$-Y \otimes Z$	$+Z \otimes I$		1	$+X \otimes I$	$+Z \otimes Z$
SWAP	0	$+I \otimes X$	$+I \otimes Z$				
	1	$+X \otimes I$	$+Z \otimes I$				

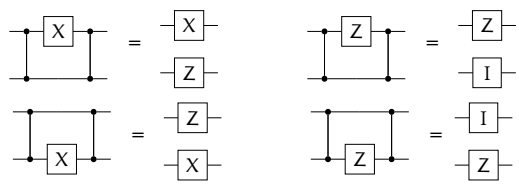

The CNOT and CZ gate are locally equivalent, and are interrelated by 1-qubit Clifford gates.

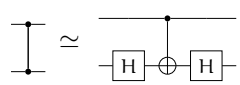

Up to local equivalence there are only 4 classes of 2-qubit Clifford gates: the 2-qubit identity; the CNOT/CZ class, iSwap/DCNOT class, and SWAP. In canonical coordinates these are $\mathrm{CAN}(0,0,0)$, $\mathrm{CAN}(\frac{1}{2},0,0)$, $\mathrm{CAN}(\frac{1}{2},\frac{1}{2},0)$, and $\mathrm{CAN}(\frac{1}{2},\frac{1}{2},\frac{1}{2})$. Any canonical gate with integer or half integer arguments is a Clifford, and can be converted to the archetype of one of the classes with 1-qubit Cliffords.

10.3 Clifford tableau

A Clifford gate can be uniquely specified by the gate's actions on the Pauli matrices. (this follows from the definition of the Clifford gates as the group that normalizes the Pauli group). And for an n qubit gate we only need to consider the action on each of the The X and Z Paulis on each of the n qubits. This is because we can deduce the action on Y from that on X and Z, and the Pauli group is factories as a direct product of single qubit Pauli. Some examples of such *Clifford tableaus* for two-qubit gates are shown fig. 4.

Table 5: Number of Clifford gates $|C_n|$ for n qubits [1]

$$|C_n| = 2^{n^2+2n} \prod_{j=1,n} 4^j - 1$$

n	$\lvert C_n \rvert$	$\log_2 \lvert C_n \rvert$	2n(2n+1)
1	24	4.58	6
2	11520	13.49	20
3	92897280	26.47	42
4	12128668876800	43.46	72
5	25410822678459187200	64.46	110
6	852437556169034724016128000	89.46	156
7	457620995529680351512370381586432000	118.46	210

The Clifford tableau representation is redundant, becuase there are additional restraints: The resultant Pauli product can't be the identity, and the X and Z actions must anti-commute (???). But the redundancy isn't large. For an n qubit gate we need to specify the action on $2n$ Paulis, each of which requires 2 bits for the 4 possibilities (I, X, Y, Z) on each qubit, plus a sign bit. So the number of bits needed to specify a Clifford is at most $2n(2n+1) \approx 4n^2$. The exact number of Clifford gates for given n is

$$|C_n| = 2^{n^2+2n} \prod_{j=1,n} 4^j - 1 \tag{99}$$

The minimum number of bits required to uniquely specific a Clifford is asymptotically $2n^2$, so the Clifford tableau redundancy is no more than a factor of 2. See table 5 for the first few numerical values.

10.4 Generation of Clifford gates

10.5 Gottesman–Knill theorem

10.6 Decomposition of Clifford gates

A Miscellaneous mathematics

A.1 Arctangent

B Weyl Chamber

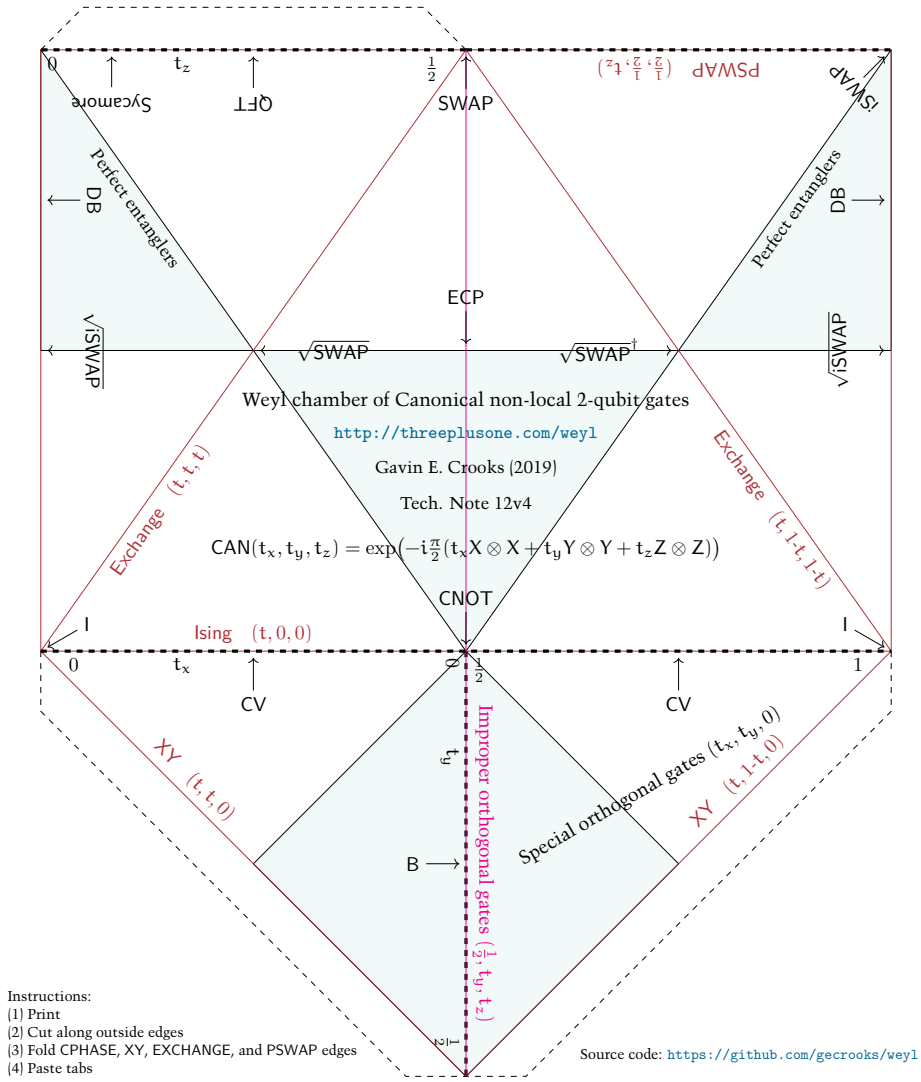

Figure 8: The Weyl chamber of canonical non-local 2 qubit gates. (Print, cut, fold, and paste)

Notes

1. And Mike and Ike.
2. The 1-qubit rotation gates are typically verbalized as *arr-ex*, *arr-why*, *arr-zee*, and *arr-en*.
3. *deke* /*dek*/ verb — To decompile, deconstruct, or decompose.
   1995 Neal Stephenson *The Diamond Age* "We gotta deke all this stuff now" Easy come, easy go.
4. The Z-Y decomposition is apparently of relatively ancient origin, long know in the theory of light polarization [**?**]
5. Open Problem: Zang et al.[29] derive the analytic decomposition of the canonical gate to a B gate sandwich only up to local gates. Derive an analytic formula for the necessary local gates to complete the canonical to B-sandwich decomposition. (page 40)

References

[1] [citation needed]. (pages 5, 6, 11, 17, 17, 23, 23, 23, 23, 25, 28, 28, 28, 28, 28, 33, 33, 33, 38, 40, 41, 41, 42, 43, 45, 45, and 51).

[2] David P. DiVincenzo. Two-bit gates are universal for quantum computation. *Phys. Rev. A*, 51:v (1995). DOI: 10.1103/PhysRevA.51.1015. ArXiv:cond-mat/9407022. (page 6).

[3] Michael A. Nielsen and Isaac L. Chuang. *Quantum Computation and Quantum Information*. Cambridge University Press (2000). (page 6).

[4] John Preskill. Quantum computation lecture notes (1997–2018). http://www.theory.caltech.edu/people/preskill/ph229/. (page 6).

[5] Leonard Susskind and Art Friedman. *Quantum Mechanics: The Theoretical Minimum*. Basic Books (2015). (page 6).

[6] J. J. Sakurai and Jim J. Napolitano. *Modern Quantum Mechanics*. Pearson, 2nd edition (2010). (page 6).

[7] Eleanor G. Rieffel. *Quantum Computing: A Gentle Introduction*. The MIT Press (2014). (pages 6 and 11).

[8] Andy Matuschak and Michael Nielsen. Quantum country (2019). https://quantum.country/. (page 6).

[9] Scott Aaronson. *Quantum Computing since Democritus*. Cambridge University Press (2013). (page 6).

[10] Ivan Savov. *No bullshit guide to linear algebra*. Minireference Co. (2017). (page 6).

[11] Sheldon Axler. *Linear Algebra Done Right*. Springer, 2nd edition (2004). (page 6).

[12] John Watrous. *The theory of quantum information*. Cambridge University Press (2018). (page 6).

[13] Mark M. Wilde. *Quantum information theory*. Cambridge University Press, 2nd edition (2017). (page 6).

[14] Chris Ferrie and whurley. *Quantum Computing for Babie*. Sourcebooks Explore (2018). (page 6).

[15] Adriano Barenco, Charles H. Bennett, Richard Cleve, David P. DiVincenzo, Norman Margolus, Peter Shor, Tycho Sleator, John A. Smolin, and Harald Weinfurter. Elementary gates for quantum computation. *Phys. Rev. A*, 52:3457–3467 (1995). DOI: 10.1103/PhysRevA.52.3457. (pages 12, 12, 13, 23, 23, 26, and 43).

[16] J. A. Jones, R. H. Hansen, and M. Mosca. Quantum logic gates and nuclear magnetic resonance pulse sequences. *Journal of Magnetic Resonance*, 135(2):353–360 (1998). arXiv:quant-ph/9805070. (page 18).

[17] C. F. Van Loan and N. Pitsianis. *Approximation with Kronecker Products*, pages 293–314. Springer Netherlands, Dordrecht (1993). ISBN 978-94-015-8196-7. DOI: 10.1007/978-94-015-8196-7_17. Van Loan–Pitsianis algorithm used to decompose Kronecker products of matrices. (page 27).

[18] Charles F. Van Loan. The ubiquitous Kronecker product. *Journal of Computational and Applied Mathematics*, 123(1):85–100 (2000). DOI: 10.1016/S0377-0427(00)00393-9. (page 27).

[19] Jun Zhang, Jiri Vala, Shankar Sastry, and K. Birgitta Whaley. Geometric theory of nonlocal two-qubit operations. *Phys. Rev. A*, 67:042313 (2003). arXiv:quant-ph/0209120. (page 28).

[20] Jun Zhang, Jiri Vala, Shankar Sastry, and K. Birgitta Whaley. Optimal quantum circuit synthesis from controlled-unitary gates. *Phys. Rev. A*, 69:042309 (2004). ArXiv:quant-ph/0308167. (page 28).

[21] M. Blaauboer and R. L. de Visser. An analytical decomposition protocol for optimal implementation of two-qubit entangling gates. *J. Phys. A : Math. Theor*, 41:395307 (2008). DOI: 10.1088/1751-8113/41/39/395307. arXiv:cond-mat/0609750. (page 28).

[22] Paul Watts, Maurice O'Connor, and Jiří Vala. Metric structure of the space of two-qubit gates, perfect entanglers and quantum control. *Entropy*, 15:1963–1984 (2013). DOI: 10.3390/e15061963. (page 28).

[23] Klaus Mølmer and Anders Sørensen. Multiparticle entanglement of hot trapped ions. *Phys. Rev. Lett.*, 82:1835–1838 (1999). (page 33).

[24] H. Häffner, C.F. Roos, and R. Blatt. Quantum computing with trapped ions. *Physics Reports*, 469(4):155–203 (2008). (page 33).

[25] Farrokh Vatan and Colin Williams. Optimal quantum circuits for general two-qubit gates. *Phys. Rev. A*, 69:032315 (2004). ArXiv:quant-ph/0308006. (page 33).

[26] S. Poletto, Jay M. Gambetta, Seth T. Merkel, John A. Smolin, Jerry M. Chow, A. D. Córcoles, George A. Keefe, Mary B. Rothwell, J. R. Rozen, D. W. Abraham, Chad Rigetti, and M. Steffen. Entanglement of two superconducting qubits in a waveguide cavity via monochromatic two-photon excitation. *Phys. Rev. Lett.*, 109:240505 (2012). (page 36).

[27] Eric C. Peterson, Gavin E. Crooks, and Robert S. Smith. Two-qubit circuit depth and the monodromy polytope. *Quantum*, 4:247 (2020). DOI: 10.22331/q-2020-03-26-247. arXiv:1904.10541. (pages 36, 36, and 40).

[28] Robert S. Smith, Michael J. Curtis, and William J. Zeng. A practical quantum instruction set architecture. ArXiv:1608.03355. (page 38).

[29] Jun Zhang, Jiri Vala, Shankar Sastry, and K. Birgitta Whaley. Minimum construction of two-qubit quantum operations. *Phys. Rev. Lett.*, 93:020502 (2004). Quant-ph/0312193. (pages 39, 40, and 54).

[30] Tommaso Toffoli. Reversible computing. In J. W. de Bakker and J. van Leeuwen, editors, *Automata, Languages and Programming, Seventh Colloquium. Noordwijkerhout, Netherlands*, pages 632–644. Springer Verlag (1980). Technical Report MIT/LCS/TM-151 (1980). Exposition of reversible classical computing, and demostration that computation can be dissipationless in principle. Origin of Toffoli (CCNOT) gate. (page 43).

[31] Edward Fredkin and Tommaso Toffoli. Conservative logic. *International Journal of Theoretical Physics*, 21(3–4):219–253 (1982). DOI: 10.1007/BF01857727. (page 43).

[32] A. Peres. Reversible logic and quantum computers. *Phys. Rev. A*, 32(6):3266–3276 (1985). DOI: 10.1103/physreva.32.3266. Origin of Peres 3-qubit gate. (page 44).

[33] David Elieser Deutsch. Quantum computational networks. *Proc. R. Soc. Lond. A*, 425(1868):73–90 (1989). (page 44 and 44).

[34] Adriano Barenco. A universal two-bit gate for quantum computation. *Proceedings of the Royal Society of London. Series A: Mathematical and Physical Sciences*, 449(1937):679–683 (1995). DOI: 10.1098/rspa.1995.0066. (page 44 and 44).

[35] Xiao-Feng Shi. Deutsch, toffoli, and cnot gates via rydberg blockade of neutral atoms. *Phys. Rev. Applied*, 9:051001 (2018). (page 44).

Index

$|+\rangle$, 20
$|-\rangle$, 20
$\pi/8$ gate, 22

bit flip, 10

Clifford gates, 22
Clifford+T, 22
computational basis, 8, 20

H, *see* Hadamard gate
Hadamard basis, 8, 20
Hadamard gate, 19
Hadamard transform, 20
Hadamard-like gates, 21, 48

I gate, *see* identity gate
identity gate, 10
Inverse T gate, 23

negation, 10
NOT, 10

octahedral group, 48

P gate, *see* S (Phase) gate
Pauli gates, commutation relations10, 10
Pauli-X gate, 10
permutation group, 48
Phase gate, *see* S gate

recursion, 58

S gate, 18

T gate, 22

Walsh-Hadamard transform, 20

X, *see* Pauli-X gate
X basis, 8
X gate, 10

Y basis, 8
Y gate, 11

Z basis, 8

Copyright © 2019-2020 Gavin E. Crooks

http://threeplusone.com/gates
Berkeley Institute for Theoretical Sciences (BITS)
typeset on 2020-11-17 with XeTeX version 0.99999
fonts: Trump Mediaeval (text), Euler (math)
2 7 1 8 2 8 1 8

This monograph is inevitably incomplete, inaccurate, and otherwise imperfect — *caveat emptor*.